UNIVERSITÀ DEGLI STUDI DI NAPOLI FEDERICO II

Dipartimento di Biologia

DOTTORATO DI RICERCA IN BIOLOGIA

XXXVIII CICLO

Unveiling CSTB-dependent molecular and cellular alterations in neuronal development in EPM1: from protein synthesis to extracellular vesicles secretion

PHD STUDENT: NATALIA ABATE

TUTOR: PROF.SSA ROSSELLA DI GIAIMO

ANNO ACCADEMICO 2024-2025

INDEX

Abstract

Unverricht–Lundborg disease (EPM1) is the most common form of progressive myoclonic epilepsy, caused by loss-of-function mutations in the *CSTB* gene. Beyond its established role as a cysteine protease inhibitor, CSTB participates in key neurodevelopmental processes, including neuronal proliferation, differentiation and synaptic plasticity. To elucidate CSTB functions and uncover mechanisms underlying EPM1 pathogenesis, we employed human iPSC-derived cerebral organoids with dorsal and ventral cortical identities to drive cell fate toward excitatory or inhibitory neuronal differentiation respectively.

At advanced maturation stages of cerebral organoids, co-immunoprecipitation and mass spectrometry analyses revealed that CSTB specifically interacts with the CCT/TRiC chaperonin complex, a regulator of cytoskeletal protein folding, translation activity and vesicle biogenesis. This interaction is specific of ventrally patterned cerebral organoids, therefore we investigated CCT-dependent processes in two experimental models derived from EPM1 iPSCs: i) ventral neural progenitor cells (vNPCs) and ii) vNPCs induced to neuronal differentiation for three days (vNPCs-D3).

Our results demonstrate that cellular alterations emerge immediately upon neuronal differentiation in EPM1 cells. Protein synthesis becomes impaired at very early stages of neuronal induction and persists throughout neuronal maturation. At early stages, EPM1 cells also exhibit fragmented actin filaments and perinuclear accumulation of late

endosome markers, indicating defective maturation of multivesicular bodies and impaired secretion of extracellular vesicles (EVs). We also reproduced EPM1 defects by silencing TCP-1, a core CCT subunit, in control neurons supporting the functional relevance of CTSB-CCT interaction.

Moreover, proteomic analysis of EVs released by EPM1 neurons during maturation revealed depletion of proteins involved in cytoskeletal organization, synaptic vesicle trafficking and calcium-dependent exocytosis.

We also investigated CSTB secretion *via* EVs using adult rat brain synaptosomes as model system and demonstrated that CSTB secretion is depolarization-dependent and regulated by extracellular and intracellular calcium balance, which also influences the secretion of CD81-positive EVs subpopulations.

Overall, this work shows that EPM1-related cellular alterations, mediated by pathological missing interaction between CSTB and CCT complex, arise at the earliest stages of neuronal differentiation. The data highlight a key role for CSTB–CCT cooperation in coordinating cytoskeletal remodeling, vesicle-mediated signaling and synaptic homeostasis, providing novel insights into EPM1 pathophysiology and potential targets for therapeutic intervention.

Chapter 1: Introduction

1.1 Progressive myoclonus epilepsies

Progressive myoclonus epilepsies (PMEs) are a group of rare genetic symptomatic epilepsies, including Unverricht‐Lundborg disease, Lafora disease, Batten disease and Neuronal ceroid lipofuscinoses (Lehesjoki et al., 1992). PMEs are characterized by myoclonus, (defined as sudden and brief involuntary muscle jerks), tonic–clonic seizures, (involving tonic stiffening followed by clonic movements), and progressive neurologic decline. The age of onset varies from infancy to adulthood, but most commonly the first symptoms start in late childhood or during adolescence. The treatment of PMEs is mainly symptomatic for the seizures and myoclonus, accompanied by supportive actions, and the prognosis varies significantly between specific disorders (Orsini et al., 2019). Unverricht–Lundborg disease (ULD or progressive myoclonic epilepsy type 1, EPM1) is one of the most common forms of PMEs. EPM1 is caused by mutations in the Cystatin B (CSTB) gene, which encodes the CSTB protein that plays a crucial role in brain development. The CSTB protein is a protease inhibitor involved in the regulation of various cellular processes in neuronal cells, including cell cycle progression, cell proliferation and differentiation, apoptosis, transcriptional activity, mitochondrial and synaptic function (Alakurtti et al., 2005; Di Giaimo, 2002; Di Matteo et al., 2020; Gorski et al., 2020; Penna et al., 2019a).

1.1.2 Molecular genetics of EPM1

EMP1 is inherited in an autosomal recessive manner and caused by biallelic mutations in the CSTB gene. CSTB is located on chromosome 21

at 21q22.3. The small gene consists of three exons that span 3 kb of genomic DNA (Figure 1)(Pennacchio et al., 1996). The gene encodes the Cystatin B protein, a cysteine protease inhibitor also known as Stefin B. Numerous CSTB mutations have been described in EPM1 patients, including missense, nonsense, frameshift and splice-site variants (Figure 1), all of which are considered to result in a loss of function. Among these variants, the most common mutation, affecting 90% of the patients, is an expansion of a unstable dodecamer repeat (5'-CCCCGCCCCGCG-3') in the promoter region of CSTB (Lalioti et al., 1997; Virtaneva et al., 1997) (Figure 1). The repeat expansion accounts for 90% of all EPM1 cases worldwide and 99% of Finnish EPM1 cases (Kälviäinen et al., 2008). In healthy individuals, two or three copies of the repeat are present, whereas EPM1-associated alleles have been reported to contain at least 30 repeat copies, with up to 80 copies detected in some patients. The expansion results in a significant reduction in the expression of the CSTB mRNA and protein in patient cells, and the loss of CSTB expression leads to the myoclonus and seizures in patients (Joensuu et al., 2007). The length of the expansion mutation may correlate with the disease onset and the severity of the myoclonus and cortical neurophysiology (Hyppönen et al., 2015).

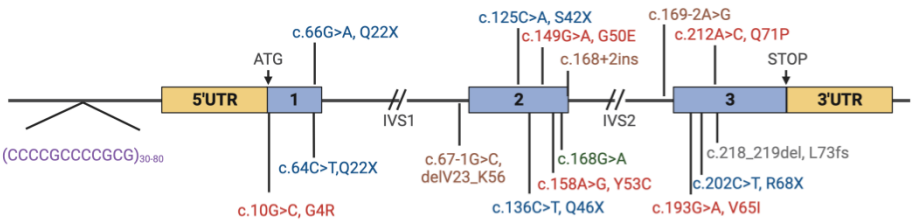

Figure 1: The structure of the CSTB gene and the locations of the reported mutations*. Red = missense mutations, blue = nonsense mutations, green = silent mutations, brown = splice site mutations, grey = frameshift mutations, purple = promoter region expansion mutation. doi.org/10.3390/cells13020170*

1.2 The CSTB protein

The CSTB protein consists of 98 amino acids and has a molecular weight of 11 kDa (Jerala et al., 1988). Protein structure is monomeric, although in cells the protein commonly exists in an oligomeric form, and the oligomerization is sensitive to redox environment (Cipollini et al., 2008). The tendency to oligomerize results in aggregate formation, and thus, the overexpression of the CSTB protein generates cytoplasmic aggregates (Cipollini et al., 2008). CSTB functions as an inhibitor of the intracellular thiol proteases, inhibiting cathepsins L, H and B as well as papain. It is considered a key player in the regulation of cellular proteostasis, protecting against proteases leaking from lysosomes (Lehesjoki and Kälviäinen, 1993), and it is suggested that it also possesses a chaperone-like function (Žerovnik, 2022).

1.2.1 CSTB expression and localization in the brain

CSTB is widely expressed in different tissues and cell types but shows different expression levels and subcellular localization in different cell types (Joensuu et al., 2008; Kopitar-Jerala, 2015). In neural cells, CSTB is expressed in embryonic and adult proliferative neural stem cells (NSCs). After the differentiation of NSCs into neurons or glial cells, the protein

levels increase further (Brännvall et al., 2003; Joensuu et al., 2008; Riccio et al., 2005). The expression pattern of Cstb protein is widely studied in rodent models, revealing dynamic changes in the rat cerebellum during development (Riccio et al., 2005). In situ hybridization and immunochemistry studies performed on adult rat brains show that the Cstb mRNA and protein are distinctly and highly expressed in the formation of hippocampal and reticular thalamic nucleus regions (D'amato et al., 2000; Joensuu et al., 2008). Moreover, Cstb mRNA is detected also in dentate gyrus cortical neurons of the hippocampus (Riccio et al., 2005). In the adult rat cerebellum, the Cstb mRNA is detected only in Purkinje cells and Bergmann fibers (Riccio et al., 2005). Similarly to rats, in humans the CSTB protein was not detectable in the whole cerebellum but was present only in Purkinje cells and Bergmann glial fibers (Riccio et al., 2005). Cstb has also been detected in the synaptic terminals isolated from rat and mouse brain cortex, and this finding was confirmed in nerve ending of human cerebral organoids (Penna et al., 2019b).

1.2.2 CSTB role in brain development

The varying distribution and localization of Cstb in neurons (Brännvall et al., 2003; Joensuu et al., 2008) suggests that it can contribute to different cellular functions in the brain. In the rat cerebellum, the Cstb protein has been shown to interact with several cytoplasmic proteins, which are known to play roles in cellular growth, proliferation and

differentiation (Di Giaimo, 2002). Two hybrid studies have shown that Cstb interacts with brain β-spectrin, a cytoskeletal protein that aids in forming different complexes and membrane domains, as well as with NF-L, neurofilament light chain, which plays a key role in the cyto-dynamics and cytoarchitecture specification (Di Giaimo, 2002; Macioce et al., 1999; Riccio et al., 2005). In addition, Cstb interacts with the cytoplasmic RACK-1 (receptor for activated C kinase 1) protein, which regulates the interaction between the cell membrane, cytoskeleton and the activated kinase (Di Giaimo, 2002; Liliental and Chang, 1998; Riccio et al., 2005). RACK-1, ß-spectrin and NF-L proteins co-localize in Purkinje cells and in Bergmann glia, where Cstb protein interacts with them, and together they guide development and differentiation (Riccio et al., 2005). In the mouse model, Cstb downregulation results in reduced neuronal proliferation and number, reduced distribution of progenitors and their premature differentiation into neurons(Forero et al., 2024b; Okuneva et al., 2015; Sierra-Torre et al., 2020). This leads to progressive atrophy as well as thinning of the cortex, and this likely underlies the cerebral ataxia. The degeneration of cortical neurons in the knockout mice takes place before any thalamic relay neuron loss (Kaasik et al., 2007; Manninen et al., 2013; Tegelberg et al., 2012). The significant reduction in the neocortex thickness is further linked with the loss of GABAergic interneurons in older mice. The reduced GABAergic terminal number and decreased ligand binding to GABA receptors in the cerebellum were observed already in presymptomatic mice, and these events were also reported in an EPM1 patient (Buzzi et al., 2012).

Several of the molecular findings from the murine model were further confirmed in a human cell model, i.e. human cerebral organoids (hCOs) generated from control and EPM1 patient iPSCs (induced pluripotent stem cells) (Di Matteo et al., 2020). In the human model, CSTB induced the recruitment of migrating interneurons in the organoids, and the level of the protein was critical in controlling progenitor cell proliferation. The overexpression of CSTB led to the expansion of progenitor cells, while a knock-down decreased the progenitor cell number. Similarly, reduced proliferation, reduced recruitment of interneurons and premature differentiation of progenitor cells were seen in the patient-derived hCOs with *CSTB* mutations (Di Matteo et al., 2020). These results from human cells show that the murine model faithfully replicates key findings from patient neurons and suggests that CSTB functions not only as a protease inhibitor but also as a key player in regulating cell proliferation, differentiation and neuronal migration. In addition to these developmental alterations, CSTB deficiency has also been associated with early microglial activation and neuroinflammatory responses. Several studies have reported that these inflammatory changes precede overt neurodegeneration in CSTB-deficient mouse models and in EPM1 patients, suggesting that neuroinflammation may contribute to disease onset and progression rather than being a mere consequence of neuronal loss (Okuneva et al., 2016, 2015; Tegelberg et al., 2012).

1.2.3 CSTB and excitatory–inhibitory imbalance

The wide expression of CSTB in different neuronal cells suggests that several neuronal types may be affected in EPM1 patients, although the loss of inhibitory neurons points to GABAergic cells as a putative target for treatment strategies. GABAergic neurons develop early during embryonic development in the cortical anlage (Chen et al., 1995). Recent studies have shown that EPM1 patients and the Cstb knockout mice have a dramatic reduction in the thickness of the cortex and a clear loss of GABAergic neurons. Electrophysiological studies showed altered GABAergic signaling, suggesting a mechanism for the latent hyperexcitability resulting in myoclonus and seizures in the patients (Buzzi et al., 2012; Franceschetti et al., 2007; Gorski et al., 2020; Joensuu et al., 2014). These alterations in inhibitory neuronal populations are recapitulated in human cerebral organoids derived from EPM1 patient iPSCs (Forero et al., 2024b). Long-term cultures of these organoids (8 months) exhibit significantly higher spontaneous neuronal activity compared to controls, characterized by a greater proportion of high-frequency spikes and overall increased firing rates (Di Matteo et al., 2025). Cellular phenotyping revealed a shift in neuronal subtype composition, with an overproduction of excitatory neurons and a concomitant reduction of inhibitory neurons, particularly in ventrally patterned organoids, which normally give rise to GABAergic interneurons. These findings collectively establish CSTB as a critical determinant of GABAergic neuron development and function, whose

disruption underlies the excitatory–inhibitory imbalance characteristic of EPM1.

1.2.4 CSTB implication in synaptic plasticity

In *Cstb* knockout mice, transcriptomic analyses revealed altered expression of genes involved in synaptogenesis (Joensuu et al., 2014). Proteomic profiling of cerebellar synaptosomes showed changes in mitochondrial, ribosomal, and intracellular transport proteins, which are essential for mitochondrial function, synaptic signaling, mRNA translation, and cytoplasmic communication (Gorski et al., 2023, 2020). These alterations suggest that the synaptic dysfunction observed in *Cstb*-deficient mice may originate from early mitochondrial impairment, leading to disrupted bioenergetics within synaptosomes. Notably, CSTB is locally synthesized in synaptosomes, and its secretion is regulated by neuronal depolarization (Penna et al., 2019). This activity-dependent release appears to play a role in the recruitment and migration of interneurons. Mechanistically, CSTB interacts with kinesin-like protein KIF1a neuron-specific motor protein of the kinesin-3 family that hydrolyzes ATP to transport cargo along microtubules from the soma to neuronal processes (Okada et al., 1995). CSTB secretion relies on KIF1a function, and in *Cstb* mutant mice, interneuron migration is perturbed compared to wild-type controls (Di Matteo et al., 2020). Importantly, these findings were observed also in human models. CSTB has been detected in synaptosomes isolated from hCOs, confirming its synaptic localization and suggesting a conserved role in synaptic function

(Pizzella et al., 2024). In hCOs derived from EPM1 patients, reduced CSTB levels correlate with decreased abundance of synaptic proteins, impaired local protein synthesis, and altered extracellular vesicle composition, pointing to a link between CSTB deficiency and disrupted synaptic plasticity in a human pathological context.

1.3 Extracellular vesicles as a cell-cell communication tools

Extracellular vesicles (EVs) are heterogeneous membrane-bound particles secreted into extracellular space by all cell types. They have emerged as critical mediators of intercellular communication, capable of transferring proteins, lipids, RNAs, and signaling molecules from donor to recipient cells (Dixson et al., 2023; Gomes et al., 2020; Raposo and Stoorvogel, 2013). The composition of EVs reflects the physiological or pathological state of the originating cells, allowing them to convey context-specific information that can modulate cellular behavior locally or at distant sites through biological fluids.

Small EVs are primarily classified into exosomes and microvesicles based on their biogenesis, size, and content. Exosomes, typically 30–200 nm, are generated within the endosomal system through inward budding of multivesicular bodies (MVBs), which fuse with the plasma membrane to release their cargo into the extracellular space (Van Niel et al., 2018). Microvesicles, larger and more heterogeneous (100–1000 nm), are produced directly by outward budding of the plasma membrane, incorporating membrane proteins and lipids from their cell of origin (Dixson et al., 2023). These structural differences confer distinct

functional capabilities to each EV subtype, influencing their interactions with recipient cells.

Importantly, EV composition changes in response to cellular stress or pathology, making them potential biomarkers for neurodegenerative disorders (Caruso Bavisotto et al., 2019).

1.3.1 Role of EVs in brain development

Brain development is a highly dynamic process involving neurogenesis, cell migration, axon guidance, and synapse formation, all of which rely on precise spatio-temporal signaling between cells (Heng et al., 2010; Rakic, 2009; Taverna et al., 2014). EVs can travel long distances, thereby mediating cell-to-cell crosstalk across diverse sites within the developing brain (Fauré et al., 2006; Patel and Weaver, 2021; Van Niel et al., 2018; Zhou et al., 2021, 2018). EVs are released by neurons (Solana-Balaguer et al., 2023; Wang et al., 2024), astrocytes (Verkhratsky et al., 2016), oligodendrocytes (Frühbeis et al., 2013), microglia (Paolicelli et al., 2019), and also by neuronal synaptic compartments (Di Giaimo et al., 2020; Olivero et al., 2021), consequently regulating diverse physiological processes, including synaptic plasticity, neurogenesis, neuronal survival, and ECM remodeling (Saeedi et al., 2019; Schiera et al., 2019; Sharma et al., 2019; Smalheiser, 2007).

Studies have shown that neural stem and progenitor cells release EVs carrying specific proteins, transcription factors, and non-coding RNAs that can influence the fate of neighboring cells. For instance, Prominin-

1 is secreted via EVs by neural stem cells, while retinal stem cells release EVs containing developmental transcription factors and microRNAs that regulate gene expression in developing mouse brain and human retinal organoids (Marzesco et al., 2005; Zhou et al., 2021). Neurons and astrocytes also secrete EVs containing adhesion molecules such as L1 and Glutamate receptor subunits, guiding neuronal differentiation and synapse formation (Fauré et al., 2006; Patel and Weaver, 2021; Takeda and Xu, 2015). Under physiological conditions, exosomes may transport the information necessary to establish correct neural connectivity and synaptic strength. For example, synaptic AMPA and NMDA glutamatergic receptors, strongly involved in long term potentiation, modulate exosomes release at synapses in differentiated neurons (Lachenal et al., 2011; Mittelbrunn et al., 2015), and synaptic glutamatergic activity and calcium influx further regulate EVs production (Lachenal et al., 2011; Saeedi et al., 2019), suggesting that some signaling molecules linked to learning and memory may be secreted via EVs (Schiera et al., 2019).

Recent studies highlight that EVs composition is highly dynamic and dependent on developmental stage, cell type and cortical regional context (Forero et al., 2024a). Proteomic profiling of human neural cells and 3D cerebral organoids revealed that EVs protein content is selectively loaded and does not directly reflect RNA expression or intraluminal vesicle composition during development (Théry et al., 2018; You et al., 2022). Notably, EVs carry physiologically functional molecules which can modulate the behavior of recipient cells.

Importantly, EVs derived from the same cell type may induce distinct responses depending on the recipient cell type, reflecting specific uptake mechanisms and intracellular localization (nuclear in neural progenitor cells, cytoplasmic in astrocytes, plasma membrane in neurons) (Hagey et al., 2023; Théry et al., 2018; Van Niel et al., 2018). Overall, these findings underscore EVs as critical mediators of non-cell-autonomous signaling in the developing human brain.

1.3.2 CSTB in extracellular vesicles: functional implications in EPM1 pathology

The modification of EVs components mirrors the change in cell and tissues, and therefore their presence in biological fluids makes them a potential diagnostic marker of Central Nervous System pathology such as neurodegenerative diseases. Moreover, dysregulation of EV-mediated signaling has been associated with neurodevelopmental disorders, including cortical malformations, autism spectrum disorders, and other forms of impaired brain connectivity (Kyrousi et al., 2021; Pipicelli et al., 2023; Sharma et al., 2019). EPM1, while not directly classified as a neurodevelopmental disorder, shares common features of neuronal dysfunction often observed in such disorders. Recent studies have shown that CSTB is present in EVs derived from 3D cerebral organoids (Figure 2A;(Forero et al., 2024b) and has also been detected in EVs secreted by synaptosomes isolated from E18 mouse brain (Figure 2B; Pizzella et al., 2024).

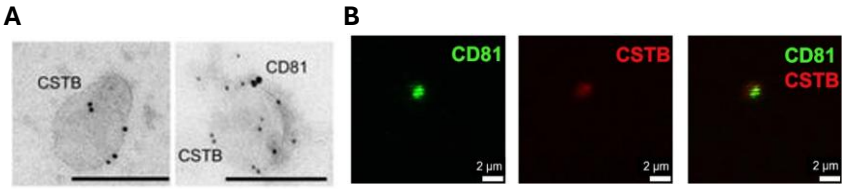

Figure 2: Presence of CSTB in EV fraction

*(**A**) Immuno-electron micrographs of CD81 (large dots) and CSTB (small dots) in EVs collected from COs. Scale bar: 1 µm. (**B**) Micrographs showing CSTB (red) and CD81-positive (green) EVs secreted from E18 mouse brain synaptosomes. Scale bar in each panel*

This dual evidence of CSTB presence in EVs secreted by cerebral organoids and rodents brain synaptosomes highlights its potential functional significance. In the context of EPM1, where CSTB is lacking, EVs exhibit alterations in biogenesis, dynamics, and molecular cargo, indicating a disruption in the processes of EVs loading and release (Forero et al., 2024b). These findings support the notion that CSTB functions not only intracellularly but also extrinsically as a mediator of neuronal signaling *via* EVs. Its absence in EPM1 may therefore compromise these mechanisms, contributing to disease pathogenesis.

1.4 Chaperonins

Proteostasis is regulated by a sophisticated network that influences the synthesis, folding, trafficking, disaggregation, and degradation of proteins. Within this network, the molecular chaperone system plays a

central coordinating role (Balchin et al., 2016). Chaperonins depend on ATP binding and hydrolysis to bind and fold non-native proteins within their enclosed central chamber (Ghozlan et al., 2022). Evolutionary, chaperonins are classified into two different groups -group I and group II- based on their architecture and folding mechanism. Group I chaperonins, which include bacterial cytosolic (GroEL), mitochondrial (HSP60) and chloroplast (Cpn60) proteins, require cochaperonins (HSP10s) to facilitate protein folding. On the other hand, the group II chaperonins consist of the archaeal chaperonins called thermosomes and the eukaryotic chaperonin named T-complex protein- 1 ring complex (TRiC/CCT) (Jin et al., 2019). TRiC/CCT either interacts directly with substrate proteins or utilises cofactors such as prefoldin and HSP70 for substrate delivery (Gestaut et al., 2023).

1.4.1 Architecture of TRiC/CCT

TRiC/CCT is a 1-MDa hetero-oligomer consisting of two stacked octameric rings that fold proteins in a manner dependent on ATP hydrolysis (Joachimiak et al., 2014). Phylogenetic analysis indicated that the different CCT subunit genes are the products of duplication events occurring early during the evolution of eukaryotic cells and that these products independently diverged with distinct functions (Archibald et al., 2000; Kubota et al., 1994). Despite sharing only 27–39% sequence identity, all CCT subunits display highly similar secondary structures, organized into three domains: the apical domain, responsible for substrate recognition and lid formation; the equatorial domain, which

harbors the ATP-binding site, and the intermediate domain, essential for ATP hydrolysis. The eight paralogous subunits forming each TRiC/CCT ring display distinct substrate recognition properties, thereby expanding the range of client proteins that can be folded. However, the activity of the complex relies on the integrity of the entire subunit ensemble: silencing a single subunit disrupts folding efficiency, reduces tubulin synthesis, and destabilizes the expression of other CCT subunits (Brackley and Grantham, 2009; Grantham et al., 2006; Pavel et al., 2016).

1.4.2 Biological functions of TRiC/CCT

As a multifunctional protein, TRiC/CCT associates with numerous partners to execute diverse functions. A central role of TRiC/CCT lies in protein synthesis and folding, where it assists nascent polypeptides in reaching their correct conformation. Recent studies have highlighted its involvement in translation initiation and elongation: for instance, it directly interacts with components of the translation initiation factor eIF3 (including eIF3b, eIF3h, and eIF3i), promoting their correct folding and functional assembly (Sha et al., 2009). Chaperone engagement with nascent chains can influence ribosome dynamics, sometimes alleviating ribosome stalling and modulating elongation rates (Goldman et al., 2015). Beyond folding, CCT also contributes to the spatial regulation of proteins within the cell, influencing their subcellular localization through lateral interactions (Hodeify et al., 2018). Notably, reduced CCT availability impairs autophagy, limiting the cell's ability to degrade

misfolded protein aggregates (Pavel et al., 2016). To compensate, alternative mechanisms such as the formation of intraluminal vesicles and secretion of extracellular vesicles (EVs) may become more prominent (Vidal et al., 1997). Several studies suggest that CCT is directly involved in the dynamics of the endolysosomal system and in EVs biogenesis (Rojas-Gómez et al., 2023). CCT has been detected in EVs derived from T lymphocytes, and its silencing results in proteomic and lipidomic reprogramming of these vesicles, indicating an active role in proteostasis via extracellular pathways (Gestaut et al., 2019; Maas et al., 2017; Martin-Cofreces et al., 2021; Van Niel et al., 2018). Importantly, CCT silencing also affects organelle homeostasis. Cells with reduced CCT display alterations in organelle number, size, and positioning, consistent with the fact that key cytoskeletal proteins, such as actin and tubulin, are obligate CCT substrates (Llorca et al., 2001, 1999; Yam et al., 2008). This suggests that CCT influences organelle dynamics and spatial organization through its role in maintaining cytoskeletal integrity. Together with its effects on organelle function, lipid metabolism, and extracellular vesicle release, these findings extend the role of CCT beyond classical proteostasis, highlighting it as a central hub coordinating cellular homeostasis at multiple levels.

1.4.3 TRiC/CCT implication in neuropathies

Increasing evidence indicates that TRiC/CCT is closely related to tumors and multiple nonmalignant diseases, such as neuropathies. These disorders share common pathogenic mechanisms, notably the failure of

the proteostasis network, which leads to the accumulation of cytotoxic protein aggregates in neurons (Hetz, 2021). In postmitotic neurons, misfolded proteins cannot be diluted through cell division, making TRiC/CCT essential for maintaining neuronal proteostasis. Dysfunction of TRiC/CCT has been observed in multiple neuropathies, including Huntington disease(Caron et al., 2018; Chen et al., 2016; Zhao et al., 2016), Parkinsons disease (Sot et al., 2017; Xie et al., 2016) and Alzheimer disease (Khabirova et al., 2014; Shen et al., 2015). Recent studies extend this perspective to neurodevelopmental diseases (Kraft et al., 2024). Observations indicate that variants in TRiC subunits can produce a wide spectrum of clinical manifestations, including relevant brain developmental disorders, suggesting that subtle perturbations in TRiC function may contribute to neurodevelopmental conditions currently classified as “idiopathic”. Analysis of individual TRiC subunits demonstrates their essential role in corticogenesis, highlighting that even partial loss-of-function or mild variants can disrupt the balance of protein folding and proteostasis during brain development. These findings support the proposal to designate TRiC-related neurodevelopmental conditions as “TRiCopathies,” emphasizing the complex’s central role in both neuronal homeostasis and proper brain formation.

Chapter 2: Aims

The expression of CSTB is finely regulated during nervous system development. Previous studies have demonstrated that CSTB is essential for interneuron migration and recruitment (Di Matteo et al.,

2020). Recent data from human cerebral organoids derived from EPM1-patient iPSCs, characterized by reduced CSTB levels, reveal cell fate alterations. Moreover, electrophysiological analyses have shown an imbalance between excitatory and inhibitory neurons, while RNA-sequencing and Immunochemistry analyses demonstrated an altered progenitor cell identity. In particular, ventral progenitors, which physiologically give rise to inhibitory GABAergic interneurons, aberrantly lost their identity and acquired dorsal-excitatory neuronal identities in EPM1 (Forero et al., 2024b). This raises the critical question of how CSTB dysfunctions perturb dorso-ventral identity specification.

Based on these observations, our **first aim** was to identify, in *ventral cortical organoids,* the physiological interactors of CSTB and the related pathways that may underline pathological features of EPM1. We performed co-immunoprecipitation analyses combined with mass spectrometry at different developmental stages, in order to uncover region- and stage-specific CSTB protein complexes potentially involved in neurodevelopmental processes affected by the disease.

Among the CSTB interactors, the CCT complex showed a strong association with CSTB in ventral organoids. This chaperonin complex is known to participate in multiple cellular mechanisms, such as protein folding autophagy and EVs secretion (Goldman et al., 2015; Pavel et al., 2016), which are commonly altered in many neuropathies (Caron et al., 2018; Shen et al., 2015; Sot et al., 2017). Then, our **second aim** was to investigate in EPM1 context, the cellular mechanisms associated with

the interaction CCT complex-CSTB, with a particular focus on protein synthesis and EVs release.

Indeed, beyond cell-autonomous defects in EPM1, cell-non-autonomous mechanisms mediated by EVs are also involved in the EPM1 pathogenesis (Forero et al., 2024b). EVs are essential mediators of intercellular communication, modulating signaling pathways that influence neural differentiation, maturation and synaptic plasticity. Recent evidence has demonstrated the presence of CSTB within EVs released by synaptosomes isolated from E18 mouse brain, supporting its role in synaptic function and highlighting the potential contribution of EV-mediated CSTB secretion to synaptic plasticity and neuronal network homeostasis (Pizzella et al., 2024).

Based on these findings, our **third aim** focused on investigating the mechanisms underlying CSTB secretion *via EVs* from synaptic terminals by using as model system the synaptosomes isolated from mature neurons in adult rat brain. We examined the role of calcium signaling and vesicular trafficking pathways in CSTB release, to better understand how CSTB contributes to synaptic function and how its dysregulation may contribute to EPM1 pathophysiology.

Chapter 3: Material and Methods

3.1 3D model: Human cerebral organoids

3.1.1 iPSCs culture

iPSCs were previously reprogrammed from 2 control lines of fibroblasts (Klaus et al., 2019) and PBMCs origin (Di Matteo et al., 2020) and from 2 EPM1 patient lines (Di Matteo et al., 2020). iPSCs were cultured on Matrigel (Corning) coated plates (Thermo Fisher, Waltham, MA, USA) in mTesR1 basic medium supplemented with 1x mTesR1 supplement (Stem Cell Technologies, Vancouver, Canada) at 37°C, 5% CO2 and ambient oxygen level. Passaging was done using Gentle Dissociation (Stem Cell Technologies) treatment.

3.1.2 Generation of dorsally- and ventrally- patterned human cerebral organoids

Reprogrammed iPSCs were used to generate patterned hCOs (Lancaster et al., 2013; Lancaster and Knoblich, 2014). On day 1, iPSCs grown to 70–80% confluency were dissociated using Accutase solution (Sigma Aldrich, St. Louis, MO, USA, A6964) treatment, counted and plated in a 96-well U-bottom plate at a density of 9,000 live cells per 150 mL in low-bFGF hESC medium with ROCK inhibitor (1:100, final concentration 50 mM) to form Embryoid Bodies (EBs). On day 4–5, EBs were transferred to neural induction medium (DMEM-F12 with 1% (v/v) N2 supplement, 1% (v/v) GlutaMAX supplement and 1% (v/v) MEM-NEAA, heparin (final concentration of 1 mgmL_1) to promote the induction of primitive neuroepithelia. After five days, during the neuronal induction, EBs were

treated individually with Smoothened Agonist (SAG) (1:10,000) (Millipore, 566660) and IWP-2 (1:2000) (Sigma-Aldrich, I0536) to promote ventral identity and with cyclopamine A (1:500) (Calbiochem, 239803) for a dorsal identity. Following 7 days, EBs were embedded in a Matrigel (Corning/VWR International, 354234) droplet. and kept in static culture in differentiation medium without vitamin A containing 1:1 mixture of DMEM/F12 and Neurobasal supplemented with 1:200 N2 supplement (Invitrogen), 1:100 B27 supplement without vitamin A (Invitrogen), 3.5 mL L21 2-mercaptoethanol, 1:4,000 insulin (Sigma), 1:100 Glutamax (Invitrogen), 1:200 MEM-NEAA. 4–5 days following the embedding, organoids were transferred to an orbital shaker in differentiation medium as above, except B27 supplement with vitamin A (Invitrogen) was used. Organoids were kept in 10-cm dishes on a shaker at 37_C, 5% CO2 and ambient oxygen level with medium changes every 3–4 days.

3.2 2D model

3.2.1 Dissociation of ventral human cerebral organoids for 2D culture

20-30 days old ventral hCOs generated from control and EPM1 iPSCs, were dissociated as previously described (Di Matteo et al., 2020), with some modifications. Briefly hCOs were dissociated to single cells using Accutase (Sigma-Aldrich, A6964). Single cells coming from a pool of two to three organoids were plated in 6-well plates in Matrigel coating with neural progenitor cells medium (NPC medium) and used for next analyses. Cells coming from a pool of four to five organoids were then

plated onto Poly-L-ornithine (10 µg/ml) (Sigma- Aldrich, P4957)/Laminin (10 µg/ml) (Sigma-Aldrich, L2020)-coated coverslips with some modifications in wells of 24-well plates (Corning) with neural progenitor cells medium (NPC medium, (Gunhanlar et al., 2018) for subsequent Immunohistochemistry analysis.

3.2.2 NPCs maintenance and early (NPCs-D3) and late (3-8 weeks) neurons generation

Neural progenitor cells (NPCs) were generated and cultured by following Basic Protocol as previously described (Zink et al., 2021), Early stages of neural differentiation (NPCs-D3) were obtained by replacing the N2B27 media (DMEM-F12 0,5%, Neurobasal 0,5%, GlutaMAX supplement 0,5%, N2 supplement 0,5%, B22 with vit A supplement 1%, Pen/Strep 1% and 2-mercaptoethanol 0,9mM) every day. Neuronal cultures were obtained from NPCs as previously described (Gunhanlar et al., 2018). Neurons were cultured for 4 and 8 weeks in the neuronal differentiation medium (Neurobasal medium: 1% N2 supplement; 2% B27 w/o vitamin A; 1% MEM-NEA; 1,25 µg/µL laminina; 1% penicillin/streptomycin, with addition of fresh 20 ng/mL BDNF, ProSpec Bio, Rehovot, Israel, 20 ng/mL GDNF, ProSpec Bio, 200 µM cAMP, Sigma-Aldrich, 1 µM ascorbic acid, Sigma-Aldrich). From week 1 to 4 the medium was changed every other day; from week 4 to 10 only half of the medium was replenished. All the cells were kept in an incubator at 37°C, 5% CO2 and ambient oxygen level with medium changes every 2–3 days.

3.2.3 EVs collection and isolation from 2D model

EVs were collected from conditioned media from neuronal cultures from 3 to 6 weeks in culture (Théry et al., 2006). We performed EV collection by the following steps: centrifugation at 300g for 10 min, supernatant centrifugation at 2000g for 10 min at 4_C, supernatant supernatant centrifugation at 100.000g for 90 min at 4_C in a fixed-angle rotor (TH865, Thermo Fisher Scientific), followed by pellet resuspension. EV pellets were finally resuspended in RIPA buffer for protein extraction. For proteomic analyses, EVs derived from 3-4-week and 5-6-week neuronal cultures were pooled to obtain sufficient protein yield.

3.3CRISPR interference (CRISPR-i)

3.3.1 CRISPR-i plasmid construct

CRISPR interference (CRISPR-i) was employed to inhibit the expression of the *TCP-1* gene, a core subunit of the CCT complex, in control vNPCs-D3. This approach allows targeted and reversible transcriptional silencing without inducing DNA double-strand breaks, by coupling a catalytically inactive Cas9 (dCas9) to the KRAB transcriptional repressor domain (Gilbert et al., 2013). KRAB transcriptional repressor will be driven to the promoter of the gene to be silenced by the guide RNA. We used a plasmid expressing the dCas9-KRAB fusion protein (pCAG-CRISPRi see map Figure 3, gift from Jaboudon lab) and a single guide RNA (sgRNA) was designed to target the *TCP-1* promoter region and cloned into the plasmid. Two single stranded oligonucleotides with

complementary sequences targeting TCP1 promoter (sgRNA-TCP1-oligo-F 5’-ACCGGTGGTCGCCGGTCGGCCGAG-3'and sgRNA-TCP1-oligo-R 5’-AAACCTCGGCCGACCGGCGACCACC-3’) were annealed by mixing equal volumes of equimolar oligonucleotides, incubated at 95°C for 5 min and slowly cooled down to room temperature. 1 µg of the CAG-CRISPRi plasmid was incubated for 2h at 37°C with *BbsI* restriction enzyme (NEB) in the appropriate buffer. Annealed Oligos were ligated into CAG-CRISPRi plasmid previously purified after enzymatic digestion. Ligation mix was used to transform chemically competent *E. coli* cells. Restriction digestion analysis and subsequent sequencing allowed to verify gRNA correct cloning.

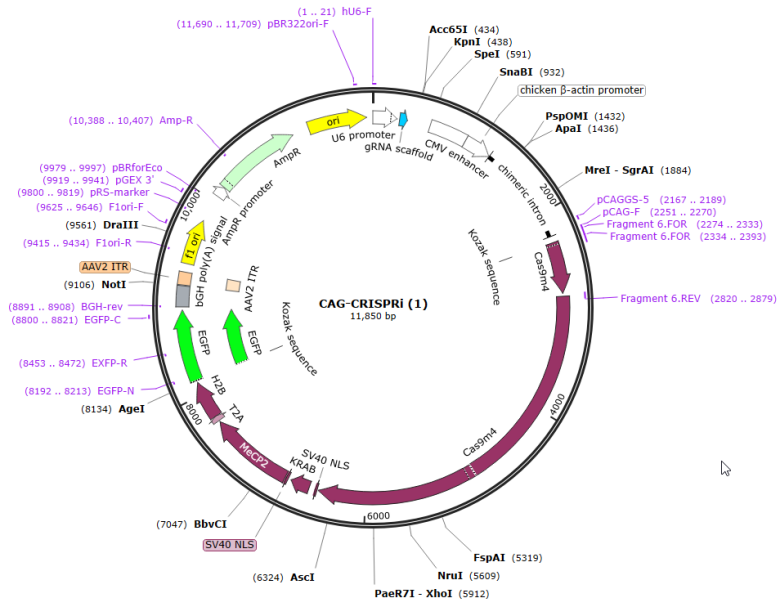

***Figure 3*: pCAG-CRISPR-i map**

3.3.2 TCP-1 silencing

vNPCs-D3 were transfected with a control plasmid expressing GFP protein to follow transfected cells (pEGFP-C1 plasmid) and TCP-1 CRISPR-i plasmid using the jetOPTIMUS DNA Transfection Reagent, Sartorius as instructed in the protocol. The fresh media were replaced 10-12h following the transfection and after three hours the conditioned media was collected for EVs collection (see EV collection and isolation). The efficiency of the transfection and relative images were then analyzed using ImageJ.60

3.4 SUrface and SEnsing of Translation (SUnSET)

vNPCs, vNPCs-D3 and mature neurons were incubated for 30 minutes with 1 µM puromycin (p8833 sigma), to detect newly synthetized protein. Cells were then rinsed with PBS and subsequently lysed in RIPA buffer. Cells were isolated by centrifugation in an Eppendorf 5415C microcentrifuge at 14,000 rpm, 5 min, 4 °C, and stored at -80 °C for subsequent western blot analysis. In addition, on 4-week control and EPM1 neurons, as well as on 8-week control neurons, puromycin incorporation was also assessed by immunofluorescence (See Immunofluorescence section), allowing visualization and quantification of protein synthesis at the single-cell level.

3.5 Immunofluorescence and imaging

Monolayer cultures were fixed with 4% paraformaldehyde for 20 mins at room temperature, followed by three 5 min washing with 1xPBS. Next, cells were blocked against unspecific binding and permeabilized in blocking buffer (10% Normal Goat Serum, 0,02% Triton-X in 1xPBS) for 1 hour. Primary antibodies diluted in blocking buffer were then added to the cells in the dilutions specified below and incubated overnight. On the second day, cells were washed three times for 5 mins each in PBS with 0,1% Tween (PBS-T) and then incubated for 2 hours in secondary antibodies raised against the host animal of the primary antibody. Secondary antibodies were diluted in blocking buffer and the dilutions used are listed below (Table 1). DAPI (4',6-diamidino-2- phenylindole) was added as a nuclear counterstaining. Finally, cells were washed three times with PBS-T and mounted on object slides with Fluoromount-G (ThermoFisher Scientific, 00-4958-02). Confocal stack images were obtained using a Leica SP8 confocal microscope based on a DMi8 stand (Leica Microsystems, Wetzlar, Germany), equipped with 20x/0.75 (oil), 40x/1.10 (water), and 63x/1.30 (glyc) objectives. Images were then processed using ImageJ (Schneider et al., 2012).

Table 1.

Puromycin	1:500	12D10 Millipore
MAP2	1:500	M4403 Merck
F-actin (Phalloidin)	1:40	A22283 Life-Technologies
RAB7	1:500	9367S Cell Signaling
Alexa Fluor_ 488 Goat Anti-mouse IgG1	1:1,000	A-21121 Life-Technologies
Alexa Fluor_ 647 Goat Anti-Rabbit IgG (H + L)	1:1,000	A-21244 Life-Technologies
Alexa Fluor_ 488 Goat Anti-mouse IgG2α	1:1,000	A-21131 Life-Technologies
Alexa Fluor_ 647 Goat Anti-mouse IgG1	1:1,000	A-21240 Life-Technologies

3.7 Animals

Wistar male rats (Charles River Laboratories, Calco, Lecco, It), of about 3 months of age, were kept in the animal house at the Department of Biology, University of Naples Federico II, Italy. All animal handling procedures were performed in accordance with European Union guidelines. Animals were kept with food and water ad libitum in a room with controlled temperature and humidity, and a 12-h light-dark regimen.

3.8 Synaptosomal fraction

3.8.1 Isolation of synaptosomal fraction from rodents cerebral cortex

Synaptosomes were prepared from cerebral cortex dissected from 3 months old rats. Synaptosomes were prepared as previously described

(Eyman et al., 2007; Penna et al., 2019). Briefly, cerebral cortices were resuspended in nine volumes of cold isotonic medium (IM: 0.32 M sucrose, 10 mM Tris-HCl, pH 7.4) and homogenized with a Dounce homogenizer. An aliquot of the homogenate was dissolved in RIPA buffer (50 mM Tris-HCl pH 8.8, 150 mM NaCl, 0.1% SDS, 0.5% NP-40, 0.5% DOC; protease and phosphatase inhibitor cocktail, Sigma-Aldrich) for subsequent analysis. The remaining homogenate was centrifuged at 2,000 x g for 1 min, 4°C. The sediment was resuspended in the same volume of IM and centrifuged again under the same conditions to remove the sediment containing nuclei, cell debris and other particulates. The two supernatants were combined and centrifuged at higher speed (23,000 x g for 4 min, 4°C) to obtain a pellet that was washed in the same volume of IM and centrifuged again as described above. The obtained pellet, named P2 fraction or crude synaptosomal fraction, contains mitochondria, myelin and synaptosomes. Synaptosomes from adult rats were further purified by discontinuous Ficoll gradient. The P2 fraction (1 mL with protein concentration of 3.2 mg/mL) was stratified on a discontinuous gradient 5-13% Ficoll in IM (2 mL each) by centrifuging at 45,000 x g for 45 min at 4°C. The purified synaptosomes were collected from the interface, diluted with nine volumes of IM and sedimented at 23,000 x g for 20 min, 4°C. The pellet was homogenized in IM and used for subsequent analyses. The protein content of both homogenate and synaptosomal fractions was determined by BIO-RAD method using bovine serum albumin (BSA) as the standard protein.

3.8.2 Incubation and isolation of extracellular vesicles from synaptosomes

Synaptosomal fraction from rodents cortices was incubated in ringer medium (90 mM NaCl, 3 mM KCl, 2 mM MgCl2, 1 mM CaCl2, 1 mM glucose, 100 mM sucrose, 30 mM Tris-HCl, pH 7.5), or in depolarizing medium (43 mM NaCl, 50 mM KCl, 2 mM MgCl2, 1 mM CaCl2, 1 mM glucose, 100 mM sucrose, 30 mM Tris-HCl, pH 7.5) or in depolarizing medium without calcium (43 mM NaCl, 50 mM KCl, 2 mM MgCl2, 1 mM glucose, 103 mM sucrose, 30 mM Tris-HCl, pH 7.5). Synaptosomes were incubated with DMSO (0,1%, vehicle of BAPTA-AM and ionomycin), or BAPTA-AM (2 µM) or ionomycin (100 nM) as indicated in the "Results" section. After 1 h incubation at 37°C, samples were cooled on ice and centrifuged at 23,000 x g for 7 min, 4°C. The resulting pellet, containing post-incubation synaptosomes, was resuspended in RIPA buffer. The supernatant, containing the secreted proteins (secretome), was further centrifuged at 100,000 x g for 2h, 4°C. The pellet, containing the ex EVs (Théry et al., 2006), was resuspended in RIPA buffer for Western Blot analysis (WB).

3.9 Nanoparticle tracking analysis

For the nanoparticle tracking analysis (NTA), fresh and frozen media from i) vNPCs-D3 transfected or not, ii) from 3 to 6 weeks neurons and iii) incubation media of synaptosomes were diluted in PBS and analyzed using a Particle Metrix ZetaView PMX110-Z Nanoparticle Tracking Analyzer (Particle Metrix GmbH, Inning am Ammersee, Germany)

equipped with a 520 nm laser. For each measurement, samples were introduced manually, the temperature was set to 24°C, and two cycles were performed by scanning at 11 discrete positions in the cell channel and capturing 60 frames per position (video setting: high). The following recommended parameters were used for the measurement.

Sensitivity: 80.0
Shutter: 70
Frame rate: 30
Minimum Brightness: 20
Minimum Area: 5
Maximum Area: 1000
Maximum Brightness: 255
Tracking Radius2: 100
Minimum Tracelength: 15
nm/class: 5
Classes/decade: 64

After capture, the videos were analyzed for particle size and concentration using the ZetaView Software 8.05.12 SP1.

3.10 Gel Electrophoresis and Western Blot analysis

Aliquots of cell lysates (vNPCs, vNPCs-D3, Neurons) and EVs isolated from synaptosomal fractions were resuspended in RIPA Buffer with protease and phosphatase inhibitor cocktail, Sigma-Aldrich. The protein samples were denatured at 100 °C for 5 min in the sample buffer (60 mM Tris-HCl pH 6.8, 10% Glycerol, 2% SDS, 100 mM DTT 0.1% bromophenol blue), separated in 10%-15% SDS-PAGE and were transferred to PVDF membranes (Merck-Millipore). The same amount

of proteins was loaded in each lane of the gel. Western blot analysis was performed as previously reported (Penna et al., 2019) with the primary antibodies indicated in table 2. After several washings in TBST, membranes were incubated with secondary antibody against rabbit (1:20,000, A0545, Sigma-Aldrich) or mouse (1:20,000, NA931, GE Healthcare) IgG linked to horseradish peroxidase. Signals were visualized by chemiluminescence (ECL, Millipore) on X-ray film (X-Ray Film, Fujifilm).

Table 2.

Puromycin	1:500	12D10 Millipore
CD81	1:500	Sc-166029 Santa Cruz
TCP1	1:10,000	ab176691 Abcam
CSTB	1:2,000	AbIN271833 Antikoerper
GAPDH	1:200,000	CB1001 Sigma-Aldrich

3.11 Co-immunoprecipitation analysis

Co-immunoprecipitation assays were performed using the Pierce™ Crosslink Magnetic IP/Co-IP Kit (Thermo Scientific, Cat. No. 88805) according to the manufacturer's instructions (Procedure for the Pierce Crosslink Magnetic IP/Co-IP Kit Manual). Dorsal and ventral cortical organoids of control derived from control iPSC lines at 20 and 40 days of differentiation, with two organoids per condition and three independent biological replicates, were collected and lysed in the lysis buffer provided with the kit (Lysis Buffer: 25mM Tris, 150mM NaCl, 1mM

EDTA, 1% NP40, 5% glycerol, pH 7.4), supplemented with 2X protease and phosphatase inhibitor cocktail (Sigma-Aldrich). For each condition, 7ug of anti-CSTB antibody (Prointech, Cat No 10823-1-AP) was covalently crosslinked to magnetic Protein A/G beads using the disuccinimidyl suberate (DSS) crosslinking reagent included in the kit to minimize antibody co-elution. Equal amounts of clarified organoid lysates were incubated with the antibody-coupled beads at RT under gentle rotation for 1h. After extensive washing, bound proteins were eluted using 110uL of elution buffer (pH 2.0) supplied with the kit, neutralized (pH 8.5), and subsequently processed for mass spectrometry analysis.

3.12 Proteomic analyses

3.12.1 Mass spectrometry

Mass spectrometry (MS) analyses were performed on protein lysates from ventral and dorsal organoids obtained after Co-IP (biological duplicates and technical triplicates) and EVs isolated from 2D neuronal cultures differentiated for 3 to 6 weeks.

Briefly, the protein extract was loaded onto the centrifugal filter CO10 kDa (Merck Millipore, Darmstadt, Germany), and detergent were removed by washing five times with 8M Urea (Merck, Darmstadt, Germany) 50mM Tris (Sigma-Aldrich, USA) buffer. Proteins were reduced by adding 5mM dithiothreitol (DTT) (Bio-Rad, Canada) at 37degrees C for 1 hour in the dark. To remove the excess of DTT, the protein sample was washed three times with 8M Urea, 50mM Tris.

Subsequently protein thiol groups were blocked with 10mM iodoacetamide (Sigma-Aldrich, USA) at RT for 45 min. Before proceeding with the enzymatic digestion, urea was removed by washing the protein suspension three times with 50mM ammonium bicarbonate (Sigma-Aldrich, Spain). Proteins were digested first by Lys-C (Promega, USA) at RT for 2 hours, then by trypsin (Premium Grade, MS Approved, SERVA, Heidelberg, Germany) at RT, overnight, both enzymes were added at an enzyme-protein ratio of 1:50 (w/w). Peptides were recovered by centrifugation followed by two additional washes with 50mM ammonium bicarbonate and 0.5M NaCl (Sigma- Aldrich, Swisserland). The two filtrates were combined, the recovered peptides were lyophilized under vacuum. Dried tryptic peptides were desalted using C18-tips (Thermo Scientific, Pierce, USA), following the manufacture instructions. Briefly, the peptides dissolved in 0.1%(v/v) formic acid (Thermo scientific, USA) were loaded onto the C18-tip and washed 10 times with 0.1 % (v/v) formic acid, subsequently the peptides were eluted by 95% (v/v) acetonitrile (Merck, Darmstadt, Germany), 0.1% (v/v) formic acid. The desalted peptides were lyophilized under vacuum. The purified peptides were reconstituted in 0.1% (v/v) formic acid for LC-MS/MS analysis.

3.12.2 MS data acquisition

Desalted peptides were loaded onto a 25 cm, 75 µm ID C18 column with integrated nanospray emitter (Odyssey/Aurora, ionopticks, Melbourne) via the autosampler of the Thermo Easy-nLC 1000 (Thermo Fisher

Scientific) at 60 °C. Eluting peptides were directly sprayed onto the timsTOF Pro (Bruker Daltonics). Peptides were loaded in buffer A (0.1% (v/v) formic acid) at 400 nl/min and percentage of buffer B (80% acetonitril, 0.1% formic acid) was ramped from 5% to 25% over 90 minutes followed by a ramp to 35% over 30 minutes then 58% over the next 5 minutes, 95% over the next 5 minutes and maintained at 95% for another 5 minutes. Data acquisition on the timsTOF Pro was performed using timsControl. The mass spectrometer was operated in data-dependent PASEF mode with one survey TIMS-MS and ten PASEF MS/MS scans per acquisition cycle. Analysis was performed in a mass scan range from 100-1700 m/z and an ion mobility range from 1/K0 = 0.85 Vs cm-2 to 1.30 Vs cm-2 using equal ion accumulation and ramp time in the dual TIMS analyzer of 100 ms each at a spectra rate of 9.43 Hz. Suitable precursor ions for MS/MS analysis were isolated in a window of 2 Th form/z < 700 and 3 Th for m/z > 700 by rapidly switching the quadrupole position in sync with the elution of precursors from the TIMS device. The collision energy was lowered as a function of ion mobility, starting from 45 eV for 1/K0 = 1.3 Vs cm-2 to 27eV for 0.85 Vs cm-2. Collision energies were interpolated linear between these two 1/K0 values and kept constant above or below these base points. Singly charged precursor ions were excluded with a polygon filter mask and further m/z and ion mobility information was used for ‘dynamic exclusion’ to avoid re-sequencing of precursors that reached a ‘target value’ of 14500 a.u. The ion mobility dimension was calibrated linearly using three ions from the Agilent ESI LC/MS tuning mix (m/z, 1/K0:

622.0289, 0.9848 Vs cm-2; 922.0097 Vs cm-2, 1.1895 Vs cm-2; 1221.9906 Vs cm-2, 1.3820 Vs cm-2).

3.12.3 Raw data analysis of MS measurements

Raw data were processed using the MaxQuant computational platform (version 1.6.17.0) (Tyanova et al., 2016) with standard settings applied for ion mobility data (Prianichnikov et al., 2020). Shortly, the peak list was searched against the Uniprot database of Human database (75069 entries, downloaded in July 2020) with an allowed precursor mass deviation of 10 ppm and an allowed fragment mass deviation of 20 ppm. MaxQuant by default enables individual peptide mass tolerances, which was used in the search. Cysteine carbamidomethylation was set as static modification, and methionine oxidation, deamidation and N-terminal acetylation as variable modifications. The matchbetween-run option was enabled, and proteins were quantified across samples using the label-free quantification algorithm in MaxQuant generating label-free quantification (LFQ) intensities.

3.12.4 Bioinformatic analyses

Bioinformatic processing and statistical analyses of proteomic data were performed using Perseus software (version 1.6.13.0, *Max Planck Institute of Biochemistry*, Munich, Germany) and RStudio (R Foundation for Statistical Computing, Vienna, Austria).

LFQ intensity values were imported into Perseus, log_2-transformed, and filtered to remove potential contaminants, reverse hits, and proteins

identified only by site. To ensure data quality, only proteins quantified in at least two of three biological replicates per condition were retained. Missing values were imputed from a normal distribution (width 0.3, downshift 1.8) to simulate low-abundance signals. Differential expression analyses were performed using two-sample *t*-tests, and proteins with $|\log_2 FC| > 0.5$ and $p < 0.05$ were considered significantly enriched. The resulting datasets were exported and further processed in RStudio for visualization and functional enrichment analyses. Volcano plots were generated using the *EnhancedVolcano* package, while Gene Ontology (GO) enrichment analyses were performed using the *clusterProfiler* and *enrichR* packages, applying an FDR threshold of 0.05. Plots were visualized with *ggplot2* and related packages within the tidyverse environment.

3.13 Statistical analysis

3.13.1 Proteomic statistical analysis

Missing values were imputed using the R package DEP (version 1.15.0) and replaced by random values of a left-shifted Gaussian distribution (shift of 1.8 units of the standard deviation and a width of 0.3). Differentially expression (DE) analysis was performed on the imputed data using Student's t Test. Proteins with log2 fold change values (log2FC) >0.5 and with an FDR-corrected q-value <0.05 were considered as differentially expressed.

3.13.2 Western Blot and Immunoflorescence statistical analysis

Statistical analyses related to WB and IF experiments were performed using GraphPad Prism 8 software. Data are presented as mean ± SEM, as indicated in the figure legends. Differences between groups were evaluated using unpaired or paired t-tests, one-way ANOVA with Tukey's post hoc test, nonparametric Mann–Whitney test, or two-way ANOVA with Sidak's post hoc test, as specified in the figure legends. A p-value < 0.05 was considered statistically significant.

Chapter 4: Results

4.1 Characterization of CSTB interactors in dorsal and ventral cortical organoids during maturation

To identify the physiological interactors of CSTB in developing human cortical regions, we performed Co-IP, followed by mass spectrometry and differential expressed proteins (DEPs) analysis, on protein lysates from dorsal and ventral cortical organoids derived from two independent control iPSCs lines, at two different developmental stages, 20 and 40 days.

At 20 days of maturation, when organoids are predominantly composed of NPCs, Co-IP analysis revealed a large overlapping set of CSTB interactors between dorsal and ventral regions (Figure 4A). This suggests that CSTB plays common roles in both regions during early stages of cortical development in human organoids.

Among these shared interactors, we identified cytoskeletal proteins such as NEFL and VIM, cysteine proteases including CTSC and CTSV, and histone proteins, some of which have already been reported as CSTB interactors in previous studies (Čeru et al., 2010; Di Giaimo, 2002)). The detection of these known CSTB partners provides an important internal validation of our experimental approach, confirming the reliability of the Co-IP/MS analysis in organoids.

At day 40 of maturation (Figure 4B), when organoids contain a mixture of NPCs and immature neurons, distinct region-specific CSTB interactors emerged. In particular, 538 proteins showed stronger interaction with

CSTB in *ventral* organoids and only 35 in *dorsal* ones (log2FC>0.5, p-value<0.05). These ventral-enriched interactors are significantly associated with biological processes including RNA splicing, translation, protein folding and cytoskeleton organization, as indicated by Gene Ontology analysis (Figure 4C). Notably, all eight subunits of the CCT complex, a key player in protein folding, cytoskeletal dynamics and vesicle biogenesis (Que et al., 2024; Rojas-Gómez et al., 2023), were detected among the top ventral-specific interactors indicating a strong interaction between CSTB and the entire CCT complex.

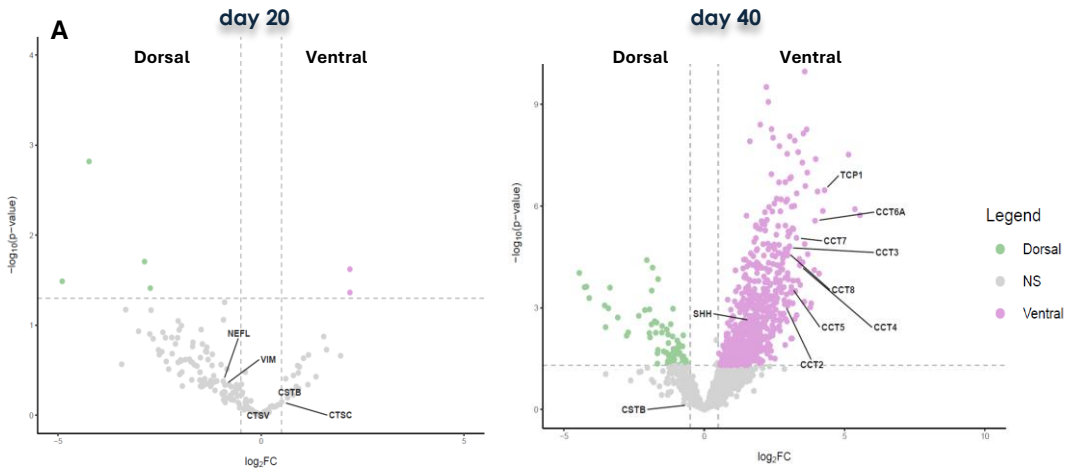

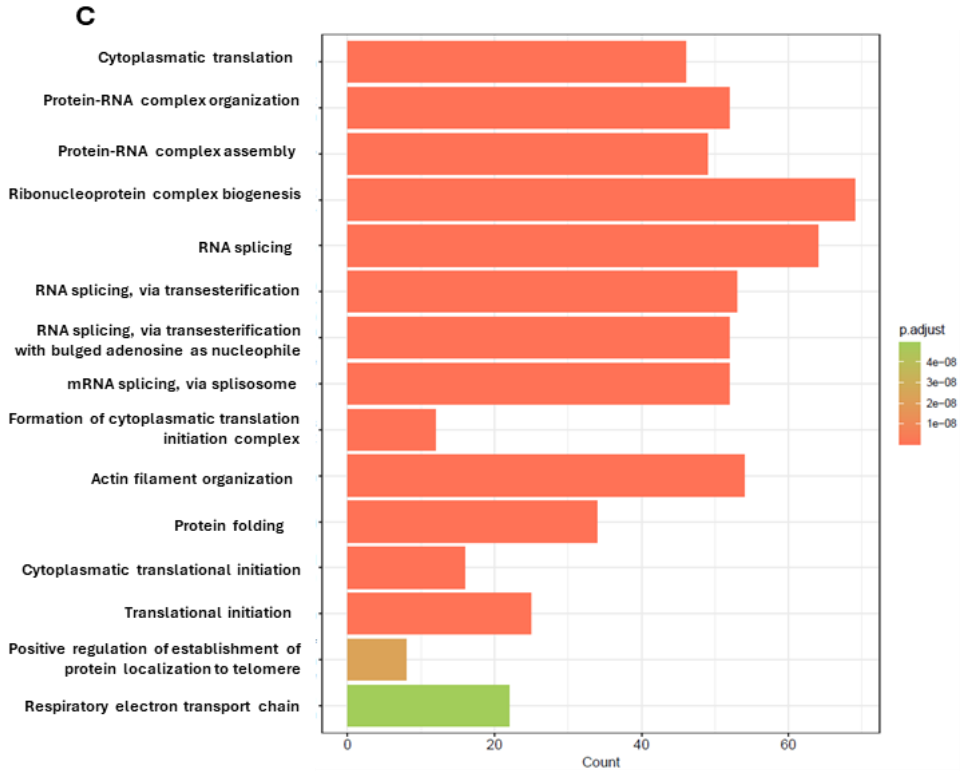

Figure 4: Temporal and regional characterization of CSTB interactors in human cerebral organoids

*(**A**) Volcano plot showing differential CSTB interactors (DEPs) between dorsal and ventral cortical organoids at day 20. Selected proteins of interest are indicated (NEFL: Neurofilament light polypeptide; VIM: Vimentin; CTSC: Cathepsin C; CTSV: Cathepsin V). (**B**) Volcano plot showing CSTB interactors (DEPs) at day 40 and the subunits of the CCT chaperonin complex (TCP1–CCT8) among the top 50 ventral-specific proteins. (**C**) Bar plot showing Gene Ontology analysis (GO) of Biological Process related to the 538 ventral-specific CSTB interactors at day 40. In volcano plots (A, B), protein levels in ventral versus dorsal cortical*

organoids are plotted as negative log10 q-values against log2 fold change. Volcano plots were generated by using EnhancedVolcano package in R studio, *significantly expressed proteins are shown (ventral: purple, log2 FC>0.5 and q < 0.05; dorsal: green, log2 FC < 0.5 and q < 0.05)*. *GO enrichment analyses were performed using the clusterProfiler and enrichR packages in R studio.*

4.2 Protein synthesis during maturation of EPM1 neurons

4.2.1 Protein synthesis impairment emerges during neuronal differentiation in EPM1 cells

Given the enrichment of CCT complex subunits among ventral-specific CSTB interactors at day 40, we next investigated whether CCT complex dependent processes are altered in ventral EPM1 cells. Due to the established role of the CCT complex in regulating protein synthesis (Goldman et al., 2015; Que et al., 2024; Sha et al., 2009), we first examined whether this process was affected in ventral EPM1 cells.

Using the SUnSET method to label newly synthetized proteins, we compared the protein synthesis levels in human EPM1 and control cells at multiple stages of maturation: ventral neuronal progenitor cells (vNPCs, Figure 5A, B), early ventral neuronal differentiation (vNPCs-D3, Figure 5C, D), and mature neurons (Figure 5E, F).

The profile of puromycin-labeled proteins showed no significant difference in protein synthesis between control and EPM1 vNPCs (Figure 5A, B). However, after only 3 days of neuronal differentiation EPM1 cells exhibited reduced protein synthesis levels compared to controls at the

same differentiation stage. (Figure 5C, D). Given the previous evidence that EPM1 cells exhibit a premature neuronal differentiation relative to controls (Di Matteo et al., 2020; Forero et al., 2024b), we extended our analysis to include control cells at a more advanced maturation stage (6 days). The persistence of the impairment of the protein synthesis levels in these conditions suggests that the defect is not merely attributable to differences in developmental timing. Figure 5C, D). Interestingly, the protein synthesis defect was maintained during development, since we observed the same results in mature neurons (Figure 5E, F). These findings indicate that protein synthesis impairment emerges during the early stages of neuronal induction and persists throughout neuronal maturation in EPM1 cells.

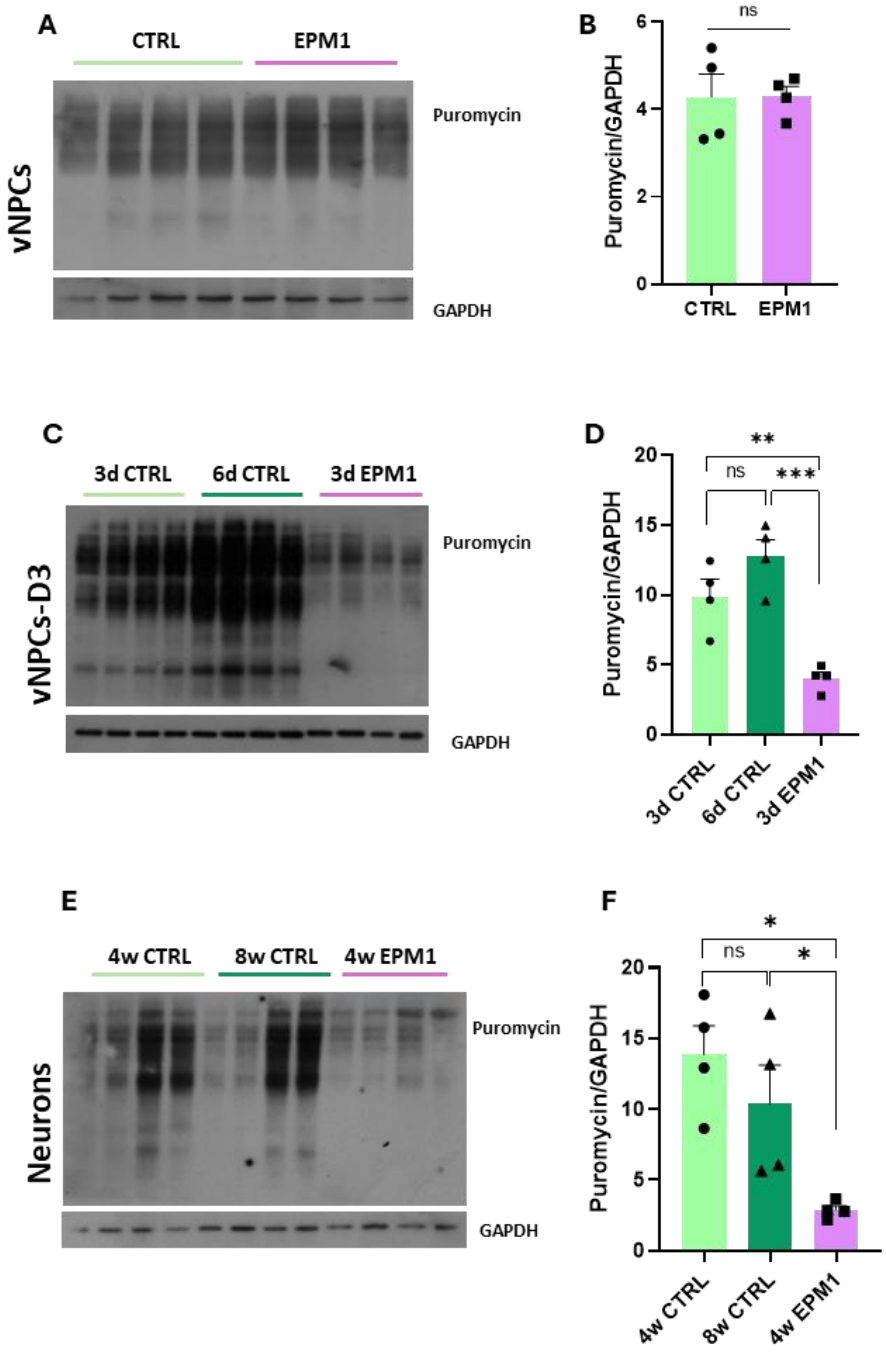
A
CTRL
EPM1
vNPCs
Puromycin
GAPDH
B
ns
Puromycin/GAPDH
6
4
2
0
CTRL
EPM1
C
3d CTRL
6d CTRL
3d EPM1
vNPCs-D3
Puromycin
GAPDH
D
**
ns
***
Puromycin/GAPDH
20
15
10
5
0
3d CTRL
6d CTRL
3d EPM1
E
4w CTRL
8w CTRL
4w EPM1
Neurons
Puromycin
GAPDH
F
*
ns
*
Puromycin/GAPDH
20
15
10
5
0
4w CTRL
8w CTRL
4w EPM1

Figure 5: Impairment of protein synthesis in EPM1 cells is dependent on maturation stage

*(**A,C,E**) Representative Western blot images showing puromycin incorporation to detect protein synthesis in: (**A**) ventral neural progenitor cells (vNPCs), **(C)** early ventral neuronal differentiation stage (vNPCs exposed to differentiation medium for 3 and 6 days (vNPCs-D3), **(E)** and mature neurons derived from control and EPM1 cells of 8 weeks of differentiation. (**B, D, F**) Corresponding quantifications of puromycin signal showed in A,C,E normalized to GAPDH as loading control. Data are presented as mean ± SEM, n=4. Statistically significant differences are assessed by Ordinary one-way ANOVA, Turkey's post hoc test, ** p value<0,01, *** p value< 0,001.*

4.2.2 Immunofluorescence confirms impaired protein synthesis in prematurely matured EPM1 neurons

To validate our Western blot findings (Figure 5), we performed SUnSET assay and immunofluorescence analysis to assess protein synthesis specifically in human mature neurons cultured in 2D for 4- and 8-weeks. Cells incubated with puromycin (in green) were stained for MAP2 (in magenta). The 4-and 8-weeks control neurons (Figure 6A-B) were compared to 4-weeks EPM1 neurons (Figure 6C) in order to account for the distinct differentiation dynamics in EPM1 cells. Quantitative analysis showed that MAP2 expression in 4-weeks EPM1 neurons was significantly higher than in 4-weeks controls and comparable to 8-weeks controls (Figure 6D), confirming the premature neuronal maturation

phenotype in EPM1 neurons (Di Matteo et al., 2020; Forero et al., 2024b). As puromycin incorporation indicated, protein synthesis levels were markedly reduced in 4-weeks EPM1 neurons compared to both 4- and 8-weeks controls (Figure 6E). After normalization of puromycin signal to MAP2 intensity, the reduction in protein synthesis remained significant, indicating a neuron-specific impairment (Figure 6F). These data, using immunofluorescence analysis, confirmed that protein synthesis deficits in EPM1 cells persist during neuronal maturation.

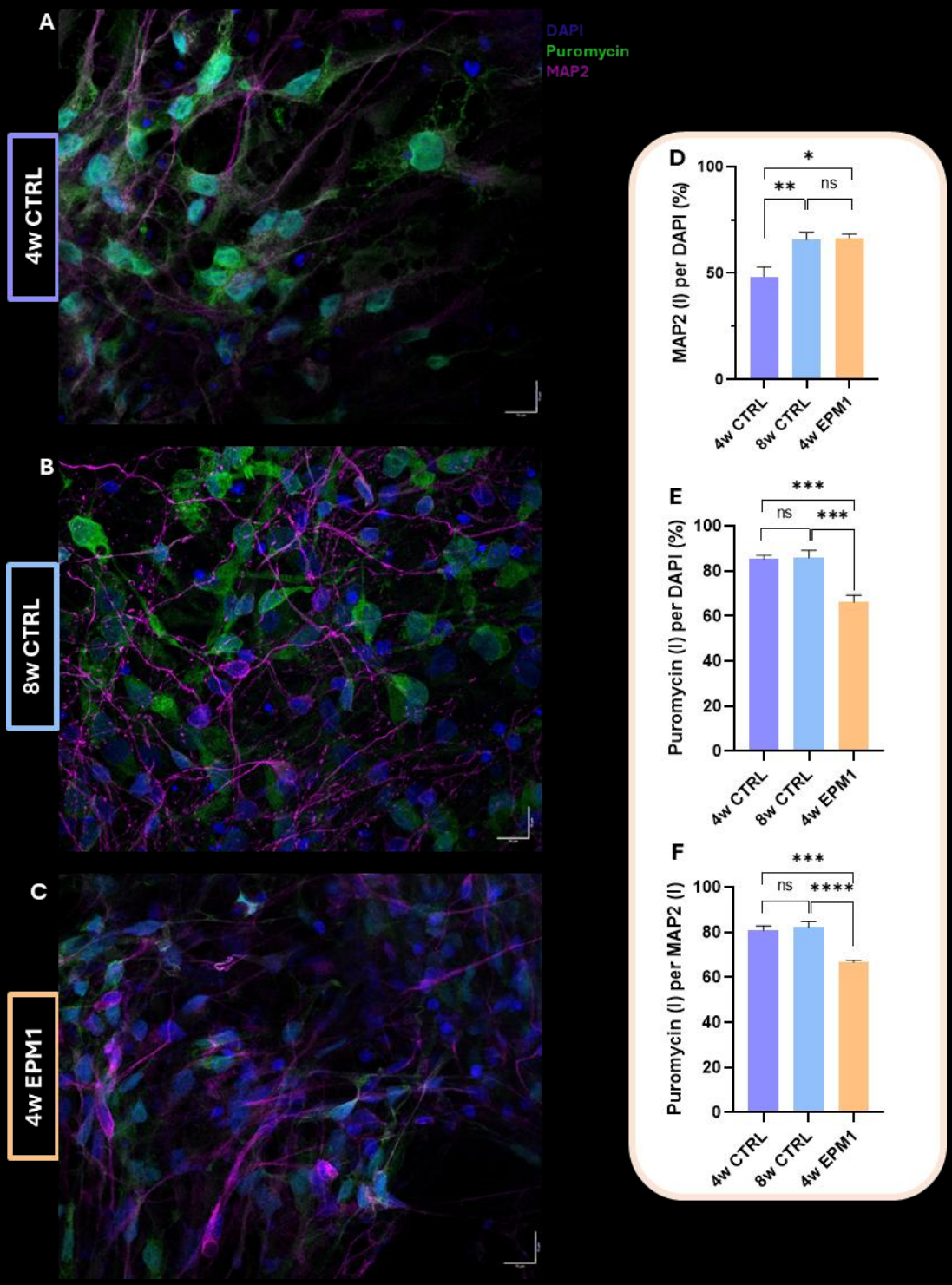
A
DAPI
Puromycin
MAP2
4w CTRL
B
8w CTRL
C
4w EPM1
D
MAP2 (l) per DAPI (%)
100
50
0
*
**
ns
4w CTRL
8w CTRL
4w EPM1
E
Puromycin (l) per DAPI (%)
100
80
60
40
20
0
***
ns
***
4w CTRL
8w CTRL
4w EPM1
F
Puromycin (l) per MAP2 (l)
100
80
60
40
20
0
***
ns
****
4w CTRL
8w CTRL
4w EPM1

Figure 6: Immunofluorescence analysis of protein synthesis in mature neurons

*(**A**) Representative immunofluorescence images showing MAP2 staining (magenta) and puromycin incorporation (green) in 4-week control neurons, (**B**) 8-week control neurons, and (**C**) 4-week EPM1 neurons.*

*(**D**) Quantification of MAP2 intensity and (**E**) puromycin incorporation normalized to the total number of DAPI-positive nuclei and presented as percentage. (**F**) Normalization of puromycin signal to MAP2 intensity confirming impaired protein synthesis specifically in neurons. Data represent mean ± SEM; n=6-7. Statistical significance determined by Ordinary one-way ANOVA, Turkey's post hoc test, *p < 0.05, **p < 0.01, *** p < 0.001, **** p < 0.0001. Scale bar: 15 µm.*

4.3 Alterations of cytoskeleton organization and endosomal pathway in EPM1

Among its many functions, CCT complex contributes to actin filament organization and to the maturation of Early Endosome and MVB, thus it has a role in extracellular vesicles production and secretion. Then, we investigated whether these CCT complex-related cellular processes are altered in EPM1.

4.3.1 Analysis of cytoskeleton and endosomal markers in vNPCs

To determine whether cytoskeletal organization or endosomal pathways are altered in patient cells at the progenitor stage, vNPCs derived from controls (Fiure 7A) and EPM1 patients (Figure 7B) were

analyzed by immunofluorescence for the presence of the late endosomal marker RAB7 (ciano) and F-actin (Phalloidin, magenta). Quantitative analysis (Figure 7C, D) revealed no significant differences in the overall signal intensity of either markers between control- and patient-derived vNPCs, indicating that both late endosomal marker expression and actin cytosckeleton organization are preserved at the progenitor stage.

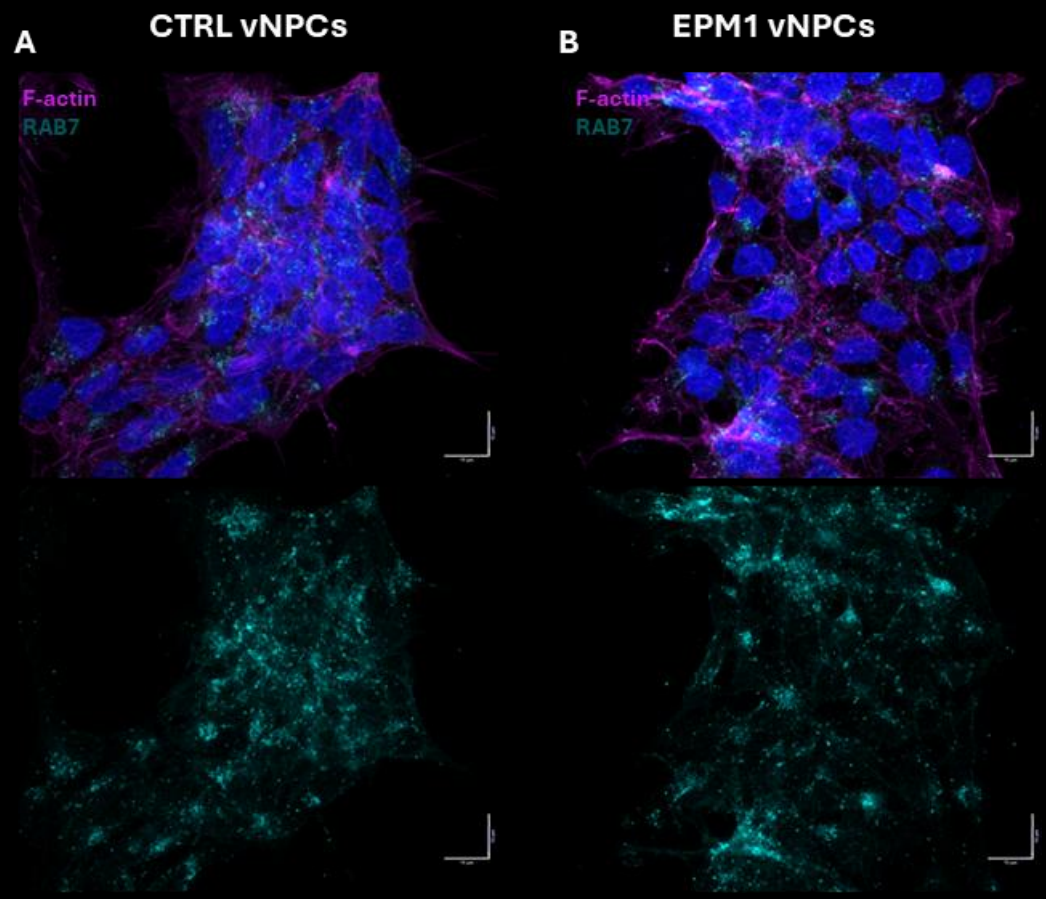
A
CTRL vNPCs
B
EPM1 vNPCs
F-actin
RAB7
F-actin
RAB7

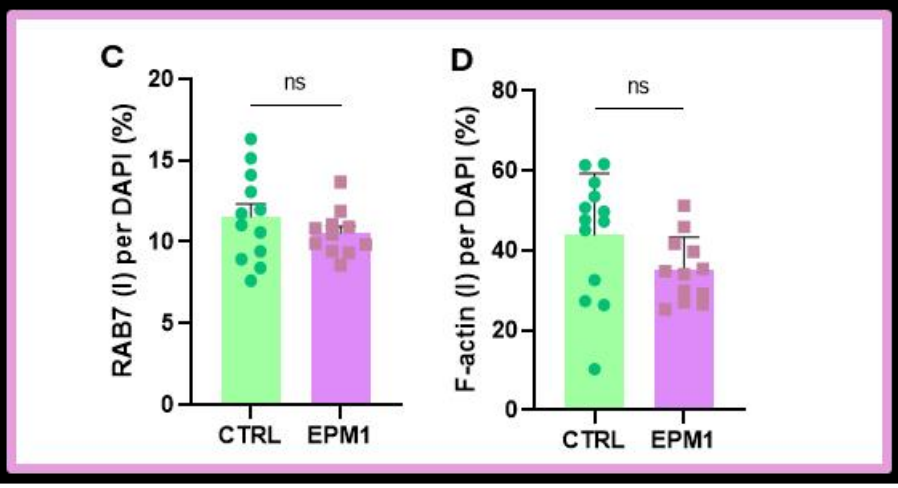
C
RAB7 (I) per DAPI (%)
20
15
10
5
0
ns
CTRL
EPM1
D
F-actin (I) per DAPI (%)
80
60
40
20
0
ns
CTRL
EPM1

Figure 7: Cytoskeletal organization and endosomal marker levels are preserved in vNPCs

Representative immunofluorescence images of ventral NPCs (vNPCs) from control (A) and EPM1 (B) cells stained for RAB7 (ciano), F-actin (phalloidin, magenta), and DAPI (blue). Quantification of RAB7 (C) and F-actin (D) fluorescence intensity normalized to the total number of DAPI-positive nuclei. Data are presented as mean ± SEM; n = 12-13 slides. Statistical analysis was performed using Unpaired t-test; ns, not significant. Scale bar: 15 µm.

4.3.2 Neuronal induction triggers cytoskeletal disorganization and perinuclear RAB7 accumulation in EPM1 ventral progenitors

Upon neuronal induction, significant changes in cytoskeletal organization and endosomal distribution became evident in EPM1 cells (Figure 8). In vNPCs-D3, overall RAB7 fluorescence intensity was comparable between control and EPM1 cells (Figure 8C), whereas quantification of its subcellular distribution revealed a significantly increased perinuclear localization in EPM1 cells compared to control ones (Figure 8D). F-actin staining showed a well-organized filamentous network in control cells (Figure 8A, E) while EPM1 cells (Figure 8B, F) exhibited a fragmented and disorganized pattern. Quantitative analysis revealed a significant decrease in actin filament length (Figure 8G) combined with an increased number of F-actin labelled segments in EPM1 cells (Figure 8H), indicating a disruption of the cytoskeletal network in EPM1 patients during early neuronal differentiation.

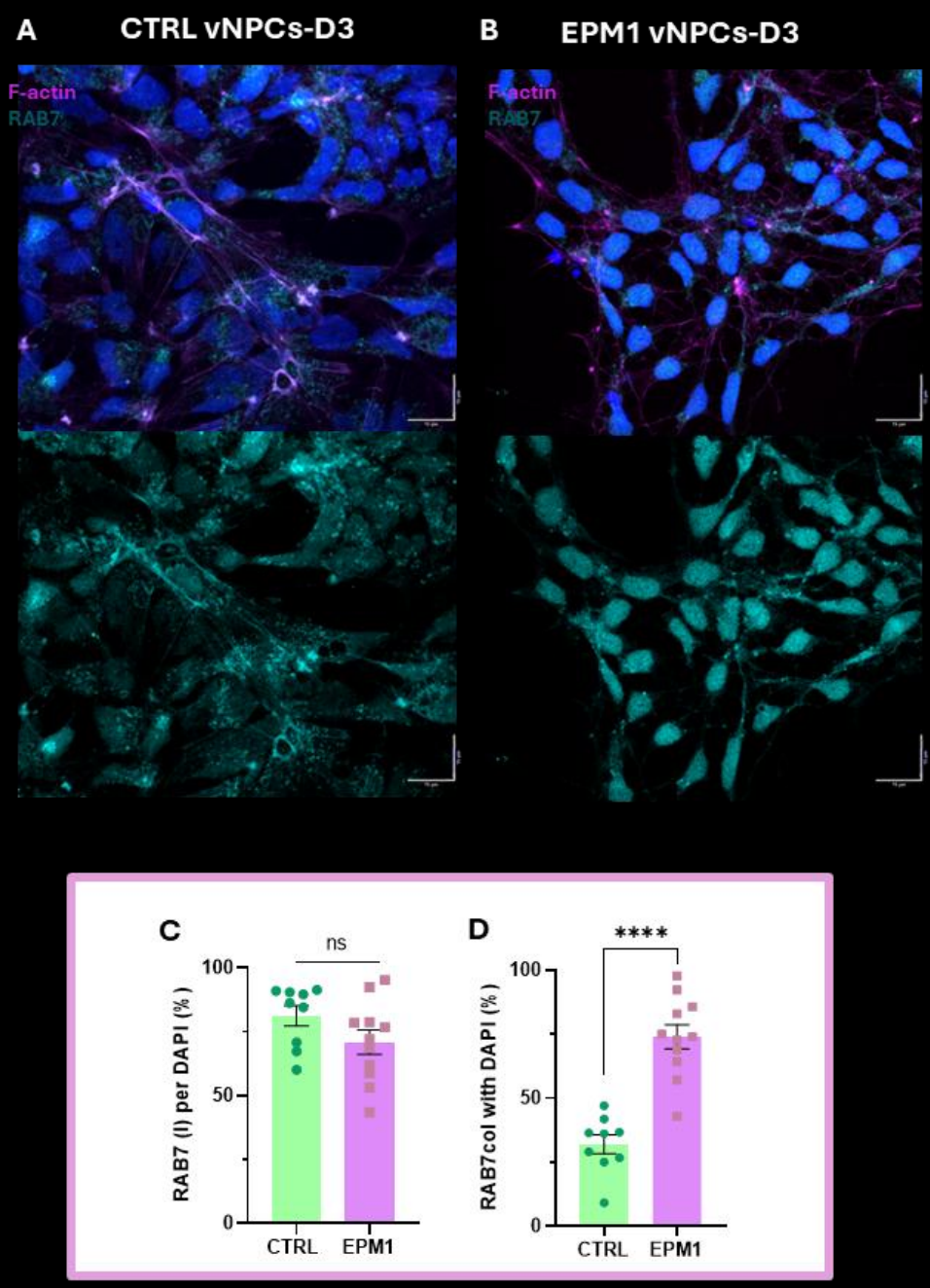
A
CTRL vNPCs-D3
B
EPM1 vNPCs-D3
F-actin
RAB7
F-actin
RAB7
C
ns
RAB7 (l) per DAPI (%)
100
50
0
CTRL
EPM1
D
****
RAB7col with DAPI (%)
100
50
0
CTRL
EPM1

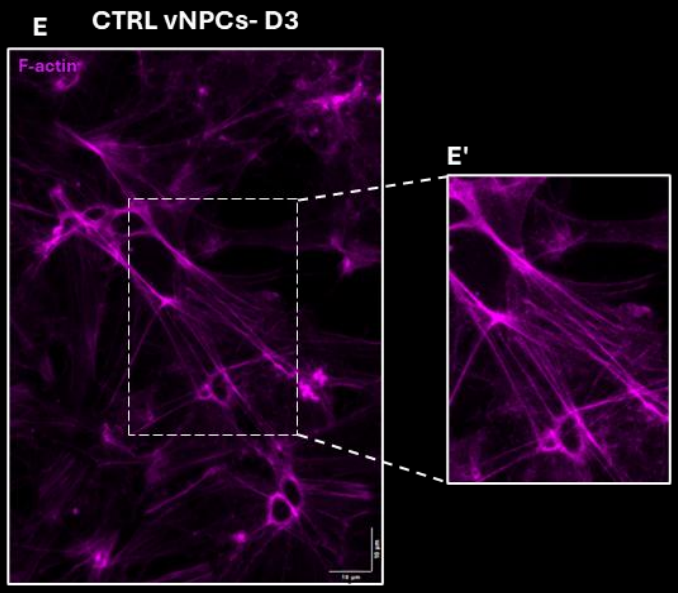
E
CTRL vNPCs- D3
F-actin
E'

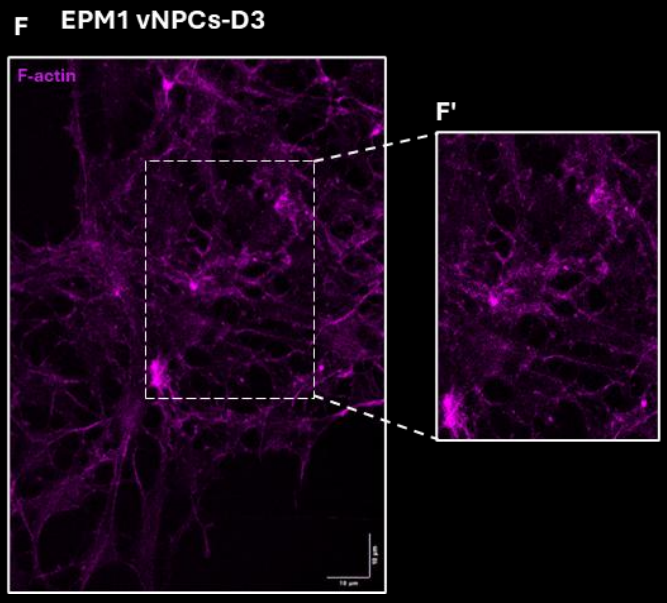
F
EPM1 vNPCs-D3
F-actin
F'

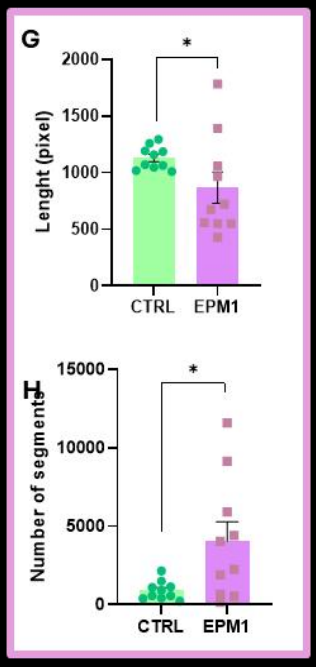
G
Lenght (pixel)
2000
1500
1000
500
0
*
CTRL
EPM1
H
Number of segments
15000
10000
5000
0
*
CTRL
EPM1

Figure 8: **Altered cytoskeletal organization and endosomal distribution in vNPCs-D3**

*(**A**) Representative immunofluorescence images of the late endosomal marker RAB7 (ciano) and F-actin (magenta) in ventral neural progenitor cells from control and (**B**) EPM1 cells after 3 days of neuronal induction (vNPCs-D3). (**C**) Quantification of total RAB7 fluorescence intensity normalized to the total number of DAPI-positive nuclei.*

*(**D**) Quantification of RAB7 colocalization with DAPI signal (blu). (**E-H**) Representative images of F-actin staining in (**E**) control and (**F**) EPM1 cells with (**E',F'**) enlarged images of the boxed area. Quantification of F-actin organization was performed by measuring (**G**) filament length and (**H**) number of segments. Data are presented as mean ± SEM; n =12-13 slides. Statistical significance determined by Unpaired t-test; ns, not significant; *p < 0.05, ****p<0.0001. Scale bar in each panel.*

4.6 Altered extracellular vesicle dynamics in early differentiation stages of EPM1 cells

CCT complex is involved in cytoskeletal dynamics and endosomal trafficking (Rojas-Gómez et al., 2023), which are essential for EVs release (Di Giaimo et al., 2020). Due to the alterations of these pathways in EPM1 cells, we assessed whether EVs release was compromised in EPM1 cells. NTA revealed that at progenitor stage (vNPCs) both the total secreted EVs number (Figure 9A) and their size distribution (Figure 9B) were comparable between control and EPM1 cells. However, following 3 days of neuronal induction, patient-derived cells released significantly fewer EVs compared to controls (Figure 9C). Additionally, EVs from EPM1 vNPCs-D3 displayed an altered size

distribution profile (Figure 9D), suggesting potential disruptions in EVs biogenesis and/or secretion mechanisms during early neuronal differentiation.

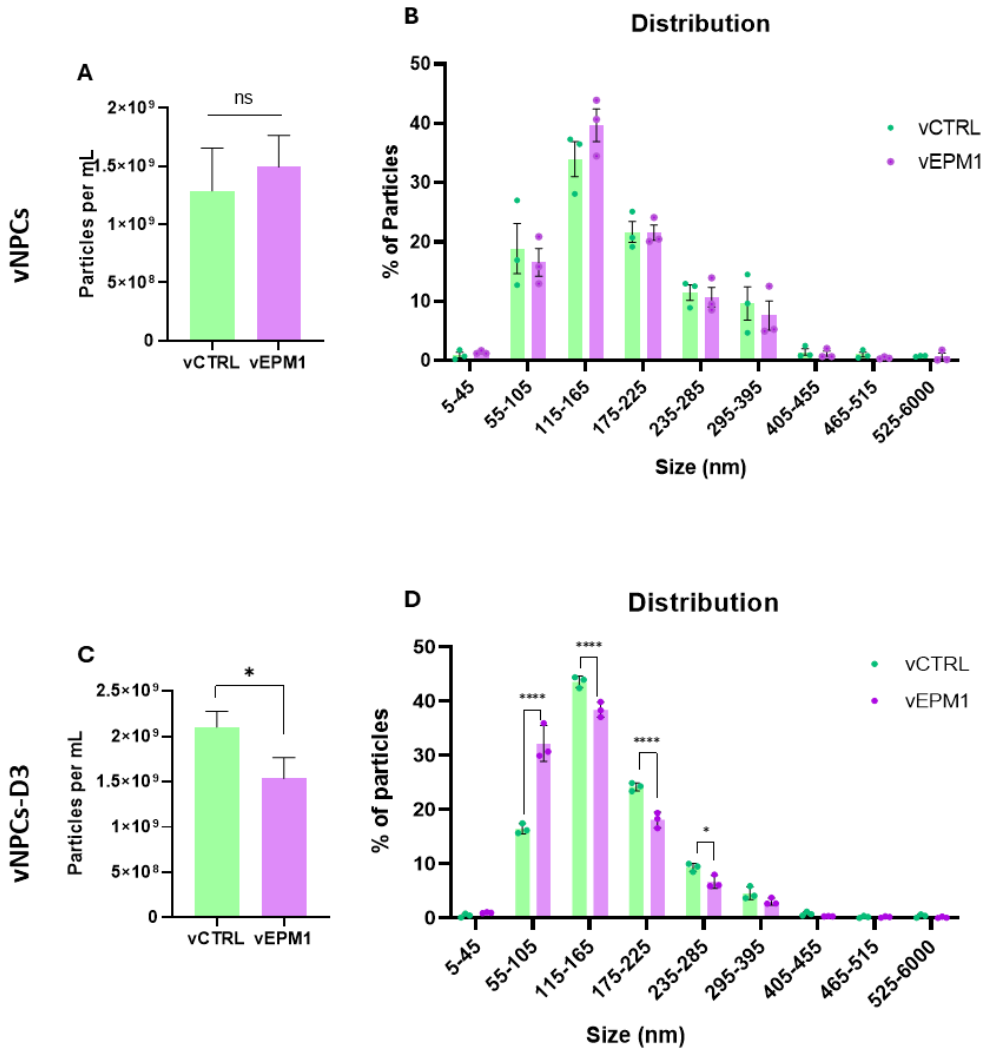

Figure 9: Nanoparticles tracking analysis (NTA) of conditioned medium from vNPCs and vNPCs-D3

*(**A**) Total number and (**B**) size distribution of EVs secreted by vNPCs from control and EPM1 cell lines. (**C**) Total number and (**D**) size distribution of EVs secreted by vNPCs* following 3 days of neuronal induction *(vNPCs-D3) from control and EPM1 cell lines. (**A, C**) Data are presented as mean ± SEM; n=3. Statistical significance was determined by Unpaired t-test; ns, not significant (**B, D**). Data are presented as mean of percentage of particles ± SEM; n=3. Statistical significance was determined by 2way ANOVA followed by Turkey's post hoc test; *p < 0.05, ****p<0.0001*

4.7 TCP-1 interference in control vNPCs-D3 mimics EVs secretion defects observed in EPM1

To functionally assess the role of the CCT complex, we silenced the TCP-1 subunit, in control vNPCs-D3 *via CRISPR interference* (CRISPR-i).

TCP-1 subunit is highly expressed in brain (Brackley and Grantham, 2009) and it is well known that the activity of the complex relies on the integrity of the entire structure (Grantham et al., 2006; Pavel et al., 2016). The experimental workflow is illustrated in Figure 10A and cell morphology after 3 days of neuronal induction is shown in Figure 10B. vNPCs-D3 were transfected with TCP1 CRISPR-i plasmid, and in parallel, under the same conditions, with a GFP-expressing plasmid to verify the efficiency of the transfection procedure (Fiure 10C) that resulted in about 20% of cells transfected. Western blot analysis (Figure 10D) and

relative quantification (Figure 10E) confirmed efficient TCP-1 interference in control vNPCs-D3 following CRISPR-i silencing.

We used the TCP-1 silenced vNPCs-D3 to investigate whether disrupted CCT structure affects EV secretion. We analyzed by NTA the conditioned media from TCP1-silenced vNPCs, and we observed a trend toward the reduction of the total number of secreted EVs compared to controls (p=0,4435), (Figure 10F). Moreover, we detected an alteration of EVs size distribution profiles with an increased number of small vesicles (45-155nm diameter) released by silenced cells compared to controls (Figure 10G). This size distribution profile, with regards to the small vesicles, resembles the pattern observed in EPM1 vNPCs-D3 (Figure 9D).

Altogether, these findings indicate that CCT complex integrity is critical for proper EVs biogenesis and release and support our hypothesis that the EVs defects observed in EPM1 may result from disrupted CSTB–CCT complex interactions.

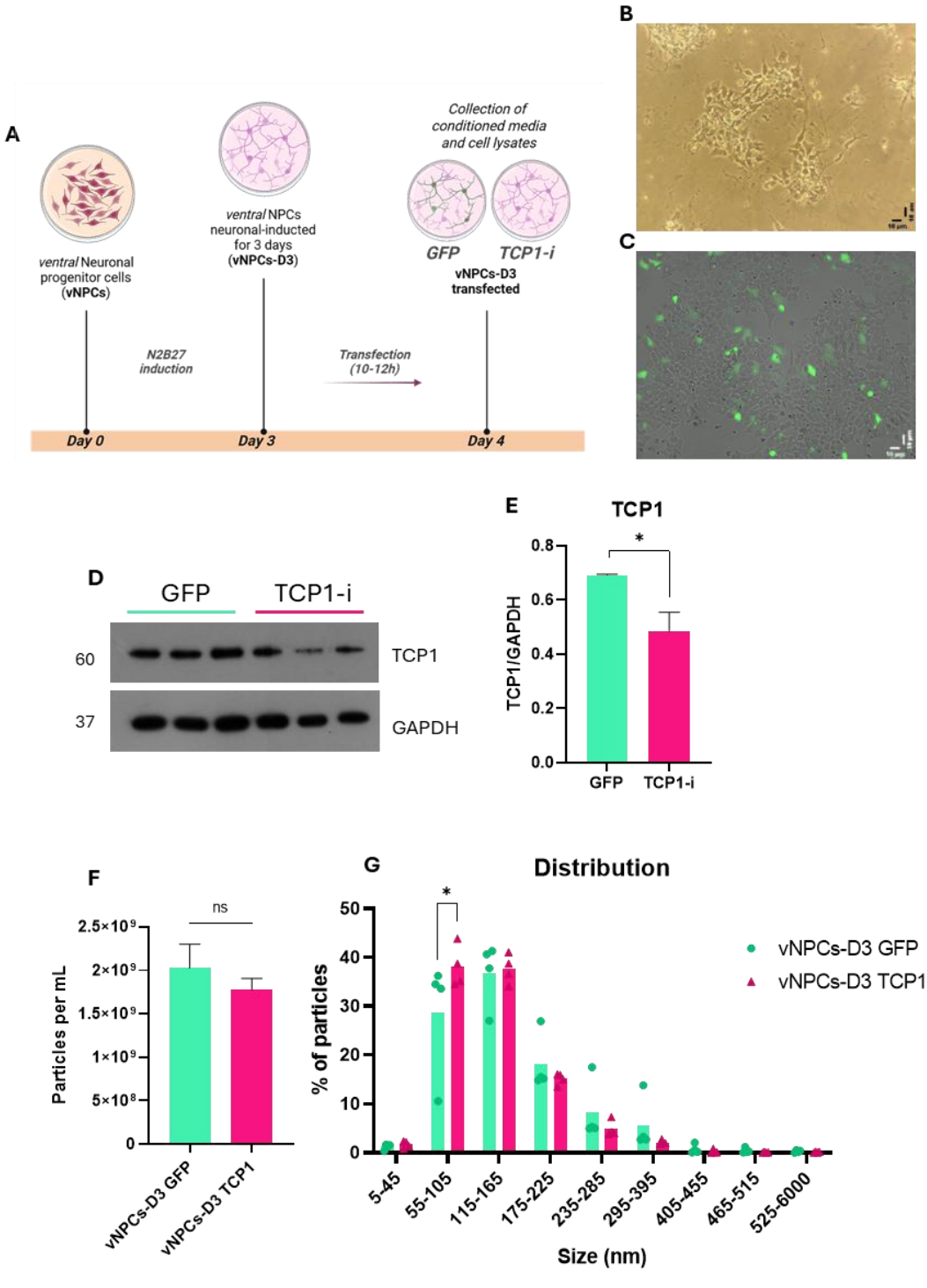
A
ventral Neuronal progenitor cells (vNPCs)
N2B27 induction
ventral NPCs neuronal-inducted for 3 days (vNPCs-D3)
Transfection (10-12h)
Collection of conditioned media and cell lysates
GFP
TCP1-i
vNPCs-D3 transfected
Day 0
Day 3
Day 4
B
C
D
GFP
TCP1-i
60
37
TCP1
GAPDH
E
TCP1
TCP1/GAPDH
0.8
0.6
0.4
0.2
0.0
GFP
TCP1-i
F
ns
Particles per mL
2.5×10⁹
2×10⁹
1.5×10⁹
1×10⁹
5×10⁸
0
vNPCs-D3 GFP
vNPCs-D3 TCP1
G
Distribution
% of particles
50
40
30
20
10
0
5-45
55-105
115-165
175-225
235-285
295-395
405-455
465-515
525-6000
Size (nm)
vNPCs-D3 GFP
vNPCs-D3 TCP1

Figure 10: Silencing of TCP1 subunit in early differentiated neurons alters extracellular vesicle release

*(**A**) Schematic representation of the experimental workflow: control vNPCs were induced towards neuronal differentiation for 3 days (vNPCs-D3), transfected with CRISPR-i plasmid targeting TCP1 gene for 10-12h, followed by a 3h recovery period before collecting cells and conditioned medium for analysis. (**B**) Representative brightfield image of vNPCs-D3 morphology prior to transfection. (**C**) Transfection efficiency control obtained by transfecting a GFP-expressing plasmid (20-30% of transfection efficiency). (**D**) Western blot analysis of TCP1 expression levels in control vNPCs-D3 after CRISPR-i–mediated silencing. (**E**) Quantification of TCP1 protein levels normalized to GAPDH. (F) Total number and (**G**) size distribution of EVs released after TCP1-silensing in control vNPCs-D3. (**E, F**) Data are presented as mean ± SEM; n=3-4. Statistical significance was determined by Unpaired t-test; ns, not significant, *p< 0.05. (**G**) Data are presented as mean of percentage of particles ± SEM; n=4. Statistical significance was determined by 2way ANOVA followed by Turkey's post hoc test; *p < 0.05. Scale bar: 10 µm.*

4.8 Persistent defects in EVs secretion and altered EVs cargo in mature EPM1 neurons

To determine whether the EVs secretion defects detected during early neuronal differentiation (Figure 9) persist at later neuronal maturation stages, we analyzed EVs released from control and EPM1 neurons at multiple differentiation stages (3, 4, and 6 weeks; Figure 11).

Conditioned media were collected every week in order to perform NTA analysis. Across all stages examined, EPM1 neurons consistently secreted fewer EVs than controls (Figure 11A) with altered size distribution (Figure 11B, C). Interestingly, the pattern shifted over maturation: the small vesicles (45-165 nm) were reduced in EPM1 neurons compared to controls, while the large ones were increased (170-400nm) (Figure 11B, C). Intrigued by these results we decided to make a qualitative analysis of vesicles protein composition. To this aim, EVs were purified from conditioned medium and proteomic analysis was performed. The volcano plot (Figure 11D), generated from DEPs across all analyzed stages, revealed, in EPM1 vesicles, a marked reduction of some proteins (406, in green), and a significant enrichment of a distinct subset of proteins in EPM1 (668, in violet). These differentially expressed proteins highlight substantial alterations in the protein content of EVs in the pathological condition.

Gene Ontology enrichment analysis of the proteins significantly enriched in EPM1 EVs (668) revealed an overrepresentation of biological processes related to inflammatory signaling, metabolic process alterations and stress response pathways (Figure 11E). These findings suggest that EVs secreted by EPM1 neurons may carry cargo associated with pathological cellular states, potentially contributing to neuroinflammation and disease progression.

Conversely, analysis of the proteins significantly reduced in EPM1 EVs (406) highlighted a strong underrepresentation of biological processes involved in actin filament organization, vesicle-mediated transport,

synaptic vesicle exocytosis, and SNARE complex assembly (Figure 11F). This depletion observed in EPM1 EVs related to proteins involved in synaptic vesicle trafficking and exocytosis confirmed the previously reported deficits of EVs synaptic secretion in EPM1 (Pizzella et al., 2024). Notably, pathways associated with calcium ion-dependent exocytosis, critical for synaptic vesicle fusion and release, were also significantly impaired.

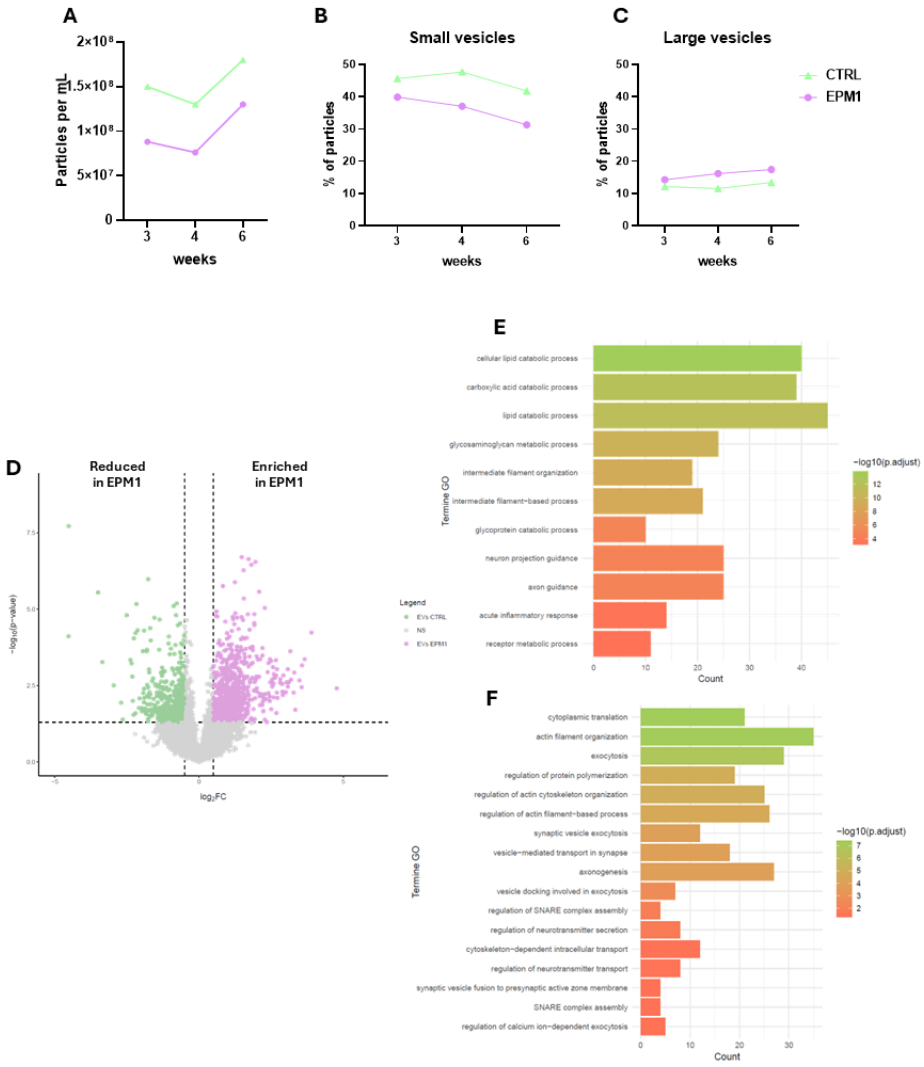

Figure 11: EVs secretion defects and cargo alterations in mature EPM1 neurons

*(**A**) NTA showing total vesicle number secreted from control and EPM1 neurons during maturation, 3-6weeks. (**B**) Distribution of small EVs in patient and control. (**C**) Distribution of large EVs in patient and control. (**D**) Volcano plot depicting differentially expressed proteins (DEPs) in patient-derived EVs versus controls, with 668 proteins significantly enriched (violet) and 406 significantly depleted (green) in EPM1 EVs. Data are plotted as negative log10 q-values against log2 fold change. Volcano plots were generated by using EnhancedVolcano package in R studio, significantly expressed proteins are shown (depleted EVs: purple, log2 FC>0.5 and q < 0.05; enriched EVs: green, log2 FC < 0.5 and q < 0.05). (**E**) Gene Ontology (GO) enrichment analysis showing biological process significantly enriched in EPM1 EVs. (**F**) GO enrichment analysis showing biological process significantly depleted in patient EVs. GO enrichment analyses were performed using the clusterProfiler and enrichR packages in R studio.*

4.9 Mechanisms of CSTB secretion from synaptic terminals of mice models: modulation by calcium ions

GO enrichment analyses revealed that synaptic vesicle cycling and calcium signaling pathways were highly impaired among EPM1-EVs proteome. CSTB has been shown to be released by rat synaptosomes in a depolarization-dependent manner (Penna et al., 2019), and CSTB secretion through EVs has been reported in human cerebral organoids

and developing mouse brain (E18). To unveil the exact mechanisms underlying CSTB release via EVs we investigated CSTB secretion under physiological conditions using synaptosomes isolated from adult rat brain, a well-established model for studying synaptic physiology. Synaptosomes are obtained by mild homogenization of brain tissue followed by subcellular fractionation, and they retain the structural and functional components of synaptic terminals *in vivo* (Whittaker, 1993). Synaptosomes were incubated into high-potassium (high-K^+) medium to induce membrane depolarization and CSTB release within the EV fraction. The CSTB-positive secreted EVs were quantified via Western Blot, comparing them with those released from synaptosomes incubated in a physiological medium (Ringer). Depolarization significantly increased CSTB expression levels in EVs fraction (Figure 12A,B). To assess whether the effect observed on CSTB was calcium-dependent, synaptosomes were also incubated in a depolarizing medium without calcium (Dep w/o Ca). Under these conditions, the depolarization-induced increase in CSTB release via EVs was reduced. These results indicate that the depolarization-dependent CSTB secretion through EVs is mediated by extracellular calcium ions, consistent with the known role of Ca^{2+} as a key regulator of vesicle exocytosis, acting through voltage-gated calcium channels that open during depolarization. In contrast, the expression levels of CD81 (an EVs marker) in EVs fraction (Figure 12C) were unaffected by depolarization, both in presence and in absence of calcium from the media. These results indicated that the extracellular calcium in depolarizing condition

is selectively affecting CSTB secretion via EVs without interfering with the secretion of CD81-positive subpopulation of EVs.

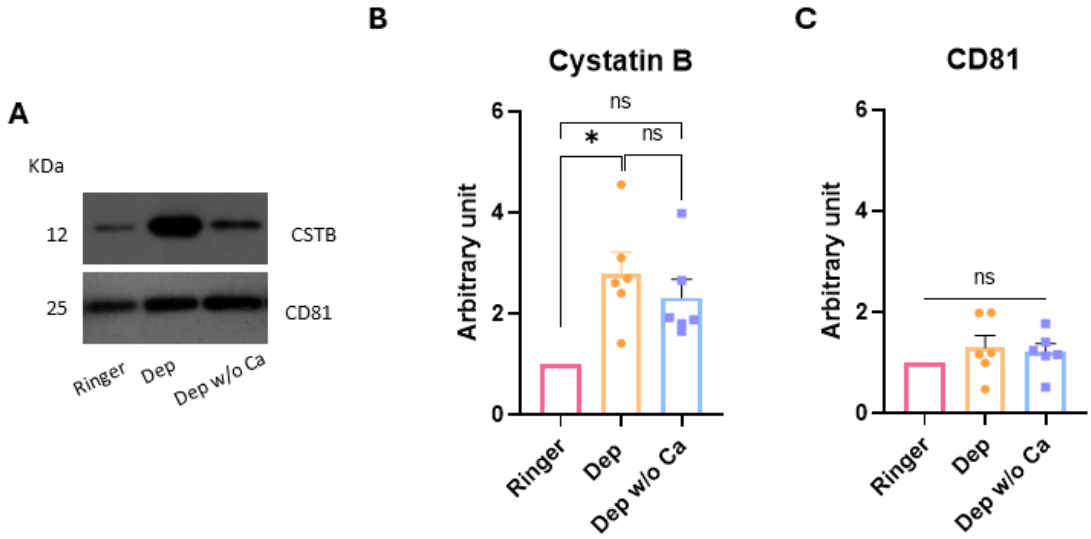

Figure 12: The depolarization-dependent CSTB secretion via EVs from rat brain cortex synaptosomes depends on extracellular calcium levels.

*(**A**) Representative images of western blot analysis. Molecular weight of each protein, in kDa, is indicated on the left. (**B**) Quantification of CSTB and (**C**) CD81 protein levels in EVs fraction secreted from rat brain cortex synaptosomes incubated in ringer medium, Dep or Dep w/o Ca. Data are presented as mean ± SEM. n=7. Statistically significant differences are based on one-way ANOVA with Tukey's post-test, ns, not significant; * p value<0.05.*

To further investigate the role of calcium ions in CSTB secretion mechanisms, we modulated intracellular calcium levels by incubating synaptosomes in the presence of BAPTA-AM, a cell-permeant calcium chelator, which decreases intracellular calcium levels, or in the presence of the calcium ionophore Ionomycin, which increases intracellular calcium levels. NTA analysis showed that BAPTA-AM did not significantly change the total number of secreted EVs (Figure 13A), whereas Western blot analysis (Figure 13B) revealed changes in EVs subtypes as suggested by CD81 expression levels (Figure 13B, C) and a reduction of CSTB levels in EVs fraction (Figure 13D). Similarly, ionomycin treatment did not alter total number of secreted EVs (Figure 13E) but decreased CSTB expression levels in EVs (Figure 13H) without significant change of CD81 levels (Figure 13F, G). Altogether, these results indicate that intracellular calcium homeostasis is required for the correct CSTB cargo and its secretion via EVs.

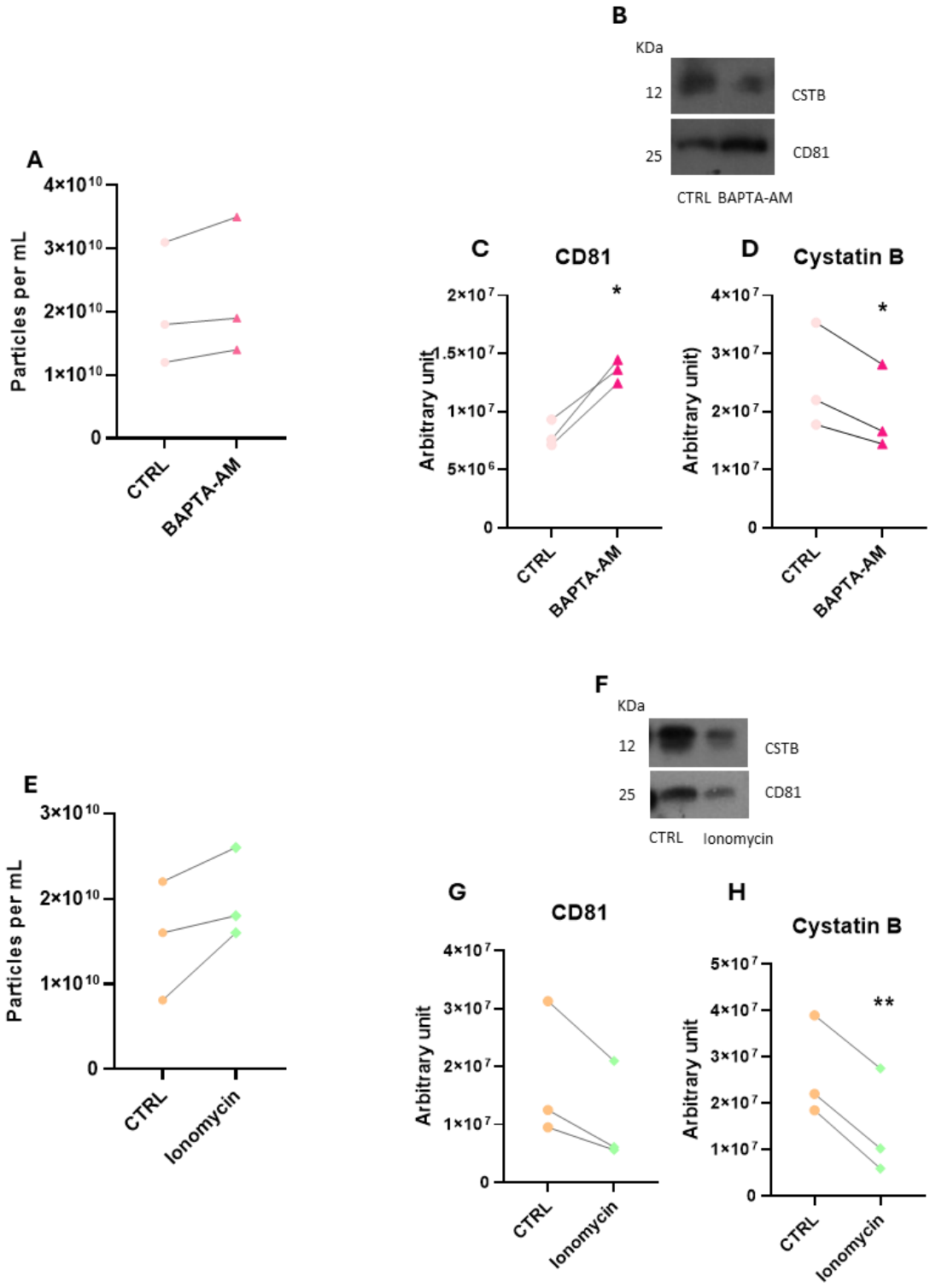
A
Particles per mL
4×10¹⁰
3×10¹⁰
2×10¹⁰
1×10¹⁰
0
CTRL
BAPTA-AM
B
KDa
12
CSTB
25
CD81
CTRL BAPTA-AM
C
CD81
Arbitrary unit
2×10⁷
1.5×10⁷
1×10⁷
5×10⁶
0
*
CTRL
BAPTA-AM
D
Cystatin B
Arbitrary unit)
4×10⁷
3×10⁷
2×10⁷
1×10⁷
0
*
CTRL
BAPTA-AM
E
Particles per mL
3×10¹⁰
2×10¹⁰
1×10¹⁰
0
CTRL
Ionomycin
F
KDa
12
CSTB
25
CD81
CTRL Ionomycin
G
CD81
Arbitrary unit
4×10⁷
3×10⁷
2×10⁷
1×10⁷
0
CTRL
Ionomycin
H
Cystatin B
Arbitrary unit
5×10⁷
4×10⁷
3×10⁷
2×10⁷
1×10⁷
0
**
CTRL
Ionomycin

Figure 13: CSTB secretion via EVs from rat brain cortex synaptosomes depends on intracellular calcium levels

*(**A**) NTA showing total number of EVs secreted from synaptosomes treated with BAPTA-AM compared to control. (**B**) Representative images of western blot analysis of EV fractions from BAPTA-AM–treated synaptosomes, showing (**C**) CD81 expression levels (**D**) CSTB content. Molecular weight of each protein, in kDa, is indicated on the left. (**E**) NTA showing total number of EVs secreted from synaptosomes treated with Ionomycin compared to control. (**F**) Representative images of western blot analysis of EV fractions from Ionomycin–treated synaptosomes, showing (**G**) CD81 expression levels (**H**) CSTB content. Molecular weight of each protein, in kDa, is indicated on the left. Data are presented as mean ± SEM. n=3. Statistically significant differences are based on Paired t-test, ns, not significant; * p value<0.05, **p<0.01.*

Chapter 5: Discussions

EPM1 is the most common form of progressive myoclonic epilepsy, caused by loss-of-function mutations in the CSTB gene (Alakurtti et al., 2005; Di Matteo et al., 2020). Studies in Cstb-knockout mice have provided important insights into disease mechanisms but structural and developmental differences between rodent and human brains limit their translational relevance (DeFelipe, 2011). To overcome this, human iPSC-derived 3D models of EPM1 disease, have been used to study neurodevelopment pathological alterations in a human-specific context (Di Matteo et al., 2020) showing that CSTB functional levels influence tangential migration and recruitment of interneurons (Di Matteo et al., 2020). Recently, electrophysiological studies performed on regionally patterned human cerebral organoids revealed an imbalance in excitatory and inhibitory neurons (Forero et al., 2024b). Moreover, RNA-sequencing and immunohistochemistry analyses demonstrated altered cell fate with ventral progenitors acquiring dorsal neuronal identities (Forero et al., 2024b). These findings suggest that CSTB plays a central role in cortical development, influencing dorso-ventral patterning.

In this project, as a first step, we performed interactome analyses revealing that in early progenitor stages, CSTB interacts with proteins involved in fundamental cellular processes, such as cytoskeletal organization, proteolysis, and chromatin regulation. These interactions are largely conserved across dorsal and ventral organoids, suggesting that CSTB initially maintains basic cellular functions that are common to all progenitors. Identified interactors such as NEFL, VIM, and NES

corroborate previous reports (Di Giaimo, 2002), while the presence of cysteine proteases and histone proteins aligns with known CSTB functions in proteolysis and gene expression regulation (Daura et al., 2022, 2021). Collectively, these data indicate that CSTB provides a stable foundation for cellular processes before the onset of region-specific differentiation programs. As corticogenesis advances, CSTB interaction networks become cortical-region-specific. By 40 days of maturation, CSTB protein partners in ventral organoids show enrichment not observed in dorsal counterparts; particularly we found all eight subunits of the CCT chaperonin complex. This ventral-specific enrichment highlights CSTB pivotal role during neuronal differentiation, possibly acting through the CCT complex, a hub for protein folding, cytoskeletal stability and vesicle trafficking (Que et al., 2024; Rojas-Gómez et al., 2023), to coordinate essential processes for ventral identity and maturation during human corticogenesis.

Based on these observations, we hypothesized that the loss of CSTB-CCT interaction in EPM1 compromises CCT-mediated functions, leading to stage-specific defects. Consistent with this hypothesis, we demonstrated that EPM1 neurons display stage-specific impairments in protein synthesis, cytoskeletal organization and vesicle-mediated processes, starting from very early neuronal differentiation. These defects likely arise from the combined effect of accelerated neuronal maturation and disrupted CSTB-CCT interactions, which compromise processes normally mediated by CCT complex. As supported by the co-immunoprecipitation analyses, these observations indicate that the first

alterations in EPM1 arise during the earliest stages of neuronal differentiation and maturation, when CSTB normally acts as a molecular trigger to orchestrate complex programs necessary for ventral cortical development.

EVs secretion plays a crucial role for intercellular crosstalk during cortical development. Indeed, vesicles carry signaling molecules essential for progenitor fate specification and regional patterning (Cederquist et al., 2019; Pipicelli et al., 2023) and aberrant EVs secretion is commonly observed in multiple neuropathies (Caron et al., 2018; Shen et al., 2015; Sot et al., 2017). Recent studies have demonstrated that CSTB is present in EVs derived from 3D cerebral organoids (Forero et al., 2024b) and has also been detected in EVs secreted by synaptic terminals isolated from E18 mouse brain (Pizzella et al., 2024), suggesting a potential functional role for CSTB in vesicle-mediated signaling. Based on these observations, we analyzed EVs release by EPM1 neurons. Following neuronal induction, EPM1-derived cells release significantly fewer EVs than controls, and these vesicles display an altered size distribution, indicating that EV-mediated intercellular communication is particularly affected in EPM1. In EPM1, these defects together with cytoskeletal and endosomal alterations, suggest that impaired vesicle biogenesis directly reflects early cellular dysfunctions.

These findings indicate that the altered pattern of EVs secretion in EPM1 neurons is likely to have functional consequences on vesicle-mediated signaling. Given that EVs carry key signaling molecules, it is reasonable

to hypothesize that disrupted EVs release could perturb the intercellular communication required for proper cortical development.

In this context, Sonic Hedgehog (SHH), a key morphogen essential for dorso-ventral patterning (Chiang et al., 1996; Fuccillo et al., 2004; Rallu et al., 2002) emerges as a particularly relevant signal. SHH is identified as a CSTB interactor in our interactome analysis in ventral organoids at day 40 of maturation, and its levels are markedly reduced in EVs secreted by EPM1 ventral organoids (Forero et al., 2024b). Reduced SHH secretion provides a mechanistic link between CSTB dysfunction, impaired EV signaling, and altered progenitor fate specification in EPM1. The involvement of the CCT complex provides a mechanistic explanation for these observations. By regulating protein folding, cytoskeletal remodeling and vesicle biogenesis, CCT enables CSTB to execute its region-specific functions during neuronal differentiation. We interfered with CCT activity, by direct silencing of the TCP-1 subunit, and reproduced EVs secretion defects as detected in EPM1 with CSTB deficiency, confirming the central role of this complex in maintaining cellular homeostasis of this process during neurogenesis. In line with previous reports, we found that silencing of CCT components alters endosomal-lysosomal dynamics, promoting multivesicular body (MVB) biogenesis and enrichment in the release of small size (45-165nm) EVs derived from intraluminal vesicles (Rojas-Gómez et al., 2023). Therefore, impaired CCT function not only compromises cytoskeletal organization but also shifts vesicle production toward smaller EVs,

consistent with the defects observed in both TCP-1 silenced and EPM1 cells.

EVs of different sizes carry distinct cargo with specific signaling roles (Zhang et al., 2023), and in EPM1 neurons, both the quantity and composition of EVs are altered. Across multiple stages of differentiation, patient-derived neurons consistently secrete fewer EVs, with a progressive shift toward larger vesicles (170-400nm), suggesting that chronic impairment of the cytoskeletal and endosomal machinery triggers adaptive remodeling of vesicle biogenesis. Proteomic profiling further revealed that EPM1 EVs carry a pathological signature: proteins related to actin filament organization, vesicle transport, synaptic vesicle exocytosis and SNARE complex assembly are depleted. These findings link early cytoskeletal defects to mature synaptic dysfunction, emphasizing how intrinsic alterations propagate to extrinsic signaling disturbances.

Moreover, the selective sensitivity of EVs cargo to intracellular and extracellular calcium levels, as demonstrated in a model system of synaptosomes from mature neurons of brain rats, highlights a finely tuned regulation of CSTB loading into vesicles that is independent of the overall EVs release. This mechanism provides a direct connection between intracellular architecture, presynaptic function, and EV-mediated signaling. Given the central role of CCT in protein folding and cytoskeletal organization, CSTB-CCT interactions likely support both the structural integrity and functional maturation of synapses, with their disruption amplifying defects in EVs cargo and synaptic communication.

These results provide a mechanistic link connecting the EV secretion defects observed in EPM1 neurons with potential alterations in synaptic vesicle biology, highlighting a plausible pathway through which disrupted CSTB–CCT interactions may contribute to impaired synaptic function in EPM1 (Pizzella et al., 2024). Notably, the reduction of EV secretion emerges as early as three days after neuronal induction and persists throughout maturation. Coupled with altered cargo composition affecting pathways essential for cell fate and synaptic function, these enduring defects point to CSTB-CCT dysfunction as a key driver of impaired EV-mediated signaling in disease. The selective sensitivity of CSTB incorporation into EVs due to calcium fluctuations in synaptosomes from mature neurons highlights a finely tuned mechanism linking intracellular signaling, presynaptic function, and EV-mediated cargo delivery. Given that CCT is a central chaperonin involved in cytoskeletal organization, it is plausible that CSTB-CCT interactions could modulate synaptic architecture and vesicle trafficking, thereby amplifying the effects of calcium-dependent sorting defects. This integrative view positions the CSTB-CCT axis as a converging point connecting intracellular structural integrity, EV-mediated communication, and synaptic homeostasis, offering a unifying framework to interpret both the synaptic and vesicular deficits observed in EPM1.

Chapter 6: Conclusions

This work provides novel insights into the molecular mechanisms underlying EPM1 pathogenesis, highlighting a novel role of CSTB in cortical development. In physiological conditions, we identified a specific interaction between CSTB and the CCT/TRiC chaperonin complex in ventral cortical patterning, linking CSTB function to fundamental cellular processes such as cytoskeletal organization, protein synthesis, vesicle production and secretion. Our findings demonstrate that alterations in these pathways arise extremely early in EPM1 context, already after three days of neuronal differentiation, indicating that the loss of CSTB impacts neuronal development from its very onset.

Proteomic studies of EVs isolated from EPM1 neurons reveal widespread deficits in synaptic pathways, particularly in synaptic vesicle trafficking and calcium-dependent exocytosis. While these alterations highlight severe functional impairments in the disease context, the physiological mechanisms of CSTB release via EVs remained unclear. Our results address this gap, showing that synaptic release of CSTB *via* EVs is a calcium-dependent and depolarization-regulated process.

Overall, these findings define the CSTB-CCT axis as a central regulator of most cellular processes, and its disruption may lead to early-onset and persistent defects in neuronal differentiation and intercellular communication.

Chapter 7: Future perspectives

Altogether, our findings strongly suggest that CSTB-CCT interactions have a central role in the emergence of EPM1-related phenotypes during early stages of neuronal differentiation, demonstrating that some of the disease alterations are specifically due to loss of this interaction. To address this, in a physiological context we have performed experiments silencing TCP-1 subunit, a core component CCT complex, which recapitulates the EVs secretion defects observed in EPM1 cells. These results support the hypothesis that disrupted CSTB-CCT interactions underlie the EPM1 phenotype.

We plan to expand our results by silencing additional CCT subunits to further validate the contribution of the entire complex. Moreover, to directly confirm that the loss of CSTB-CCT interaction drives the pathological phenotype, we plan to reintroduce CSTB in EPM1 cells and assess whether this rescue of the defects in cytoskeletal organization, EVs secretion and protein synthesis. Finally, combined experiments involving CSTB reintroduction together with CCT silencing will allow us to dissect the dependency of these processes on CSTB-CCT interactions and definitively establish a causal link.

These experiments will not only provide mechanistic validation of the CSTB-CCT axis in EPM1 pathophysiology but also broaden our understanding of CSTB functions in brain development and open new avenues for potential therapeutic approaches.

Chapter 8: Limitation of the study

Despite the relevance of the results presented in this thesis, some limitations should be acknowledged. First, the transfection efficiency achieved in the experiments was relatively low and was not directly quantified. This is likely related to the intrinsic resistance of the cellular model to conventional transfection methods, which may have contributed to variability across experiments. The use of constructs co-expressing a fluorescent reporter (e.g., GFP) would enable a more accurate and direct assessment of transfection efficiency in future studies. In addition, the adoption of alternative delivery approaches with higher efficiency, such as nucleofection-based systems (e.g., Amaxa), could substantially improve transgene delivery and reduce experimental variability. Second, although CRISPR-based approaches were instrumental in addressing the research questions of this study, potential off-target effects cannot be completely excluded. Future studies employing independent guide RNAs and complementary experimental strategies will be required to further validate the specificity of the observed effects. Finally, the ex vivo analysis of synaptosome-derived extracellular vesicle secretion was not extended to the EPM1 condition. Expanding this approach to EPM1 samples will be important to assess the relevance of these findings in the pathological context.

Chapter 9: ACRONIMYS

Co-IP *Co-immunoprecipitation*
CRISPR-i *CRISPR interference*
CSTB *cystatin B*

EPM1 *Myoclonic epilepsy type 1*
EVs *extracellular vesicles*

hCOs *human cerebral organoids*

iPSCs *induced pluripotent stem cells*

MVBs *multivesicular bodies*

NTA *Nanotracking analysis*

PMEs *Progressive myoclonus epilepsies*

SUnSET *surface and sensing of translation*

TRiC/CCT *T-complex protein- 1 ring complex*

vNPCs *ventral neuronal progenitor cells*
vNPCs-D3 *ventral neuronal progenitor cells after three days of neuronal induction*

Chapter 10: References

Alakurtti, K., Weber, E., Rinne, R., Theil, G., Haan, G.-J.D., Lindhout, D., Salmikangas, P., Saukko, P., Lahtinen, U., Lehesjoki, A.-E., 2005. Loss of lysosomal association of cystatin B proteins representing progressive myoclonus epilepsy, EPM1, mutations. Eur J Hum Genet 13, 208–215. https://doi.org/10.1038/sj.ejhg.5201300

Archibald, J.M., Logsdon Jr., J.M., Doolittle, W.F., 2000. Origin and Evolution of Eukaryotic Chaperonins: Phylogenetic Evidence for Ancient Duplications in CCT Genes. Molecular Biology and Evolution 17, 1456–1466. https://doi.org/10.1093/oxfordjournals.molbev.a026246

Balchin, D., Hayer-Hartl, M., Hartl, F.U., 2016. In vivo aspects of protein folding and quality control. Science 353, aac4354. https://doi.org/10.1126/science.aac4354

Brackley, K.I., Grantham, J., 2009. Activities of the chaperonin containing TCP-1 (CCT): implications for cell cycle progression and cytoskeletal organisation. Cell Stress and Chaperones 14, 23–31. https://doi.org/10.1007/s12192-008-0057-x

Brännvall, K., Hjelm, H., Korhonen, L., Lahtinen, U., Lehesjoki, A.-E., Lindholm, D., 2003. Cystatin-B is expressed by neural stem cells and by differentiated neurons and astrocytes. Biochemical and Biophysical Research Communications 308, 369–374. https://doi.org/10.1016/S0006-291X(03)01386-X

Buzzi, A., Chikhladze, M., Falcicchia, C., Paradiso, B., Lanza, G., Soukupova, M., Marti, M., Morari, M., Franceschetti, S., Simonato, M., 2012. Loss of cortical GABA terminals in Unverricht–Lundborg disease. Neurobiology of Disease 47, 216–224. https://doi.org/10.1016/j.nbd.2012.04.005

Caron, N.S., Dorsey, E.R., Hayden, M.R., 2018. Therapeutic approaches to Huntington disease: from the bench to the clinic. Nat Rev Drug Discov 17, 729–750. https://doi.org/10.1038/nrd.2018.133

Caruso Bavisotto, C., Scalia, F., Marino Gammazza, A., Carlisi, D., Bucchieri, F., Conway De Macario, E., Macario, A.J.L., Cappello, F., Campanella, C., 2019. Extracellular Vesicle-Mediated Cell–Cell

Communication in the Nervous System: Focus on Neurological Diseases. IJMS 20, 434. https://doi.org/10.3390/ijms20020434

Cederquist, G.Y., Asciolla, J.J., Tchieu, J., Walsh, R.M., Cornacchia, D., Resh, M.D., Studer, L., 2019. Specification of positional identity in forebrain organoids. Nat Biotechnol 37, 436–444. https://doi.org/10.1038/s41587-019-0085-3

Čeru, S., Konjar, Š., Maher, K., Repnik, U., Križaj, I., Benčina, M., Renko, M., Nepveu, A., Žerovnik, E., Turk, B., Kopitar-Jerala, N., 2010. Stefin B Interacts with Histones and Cathepsin L in the Nucleus. Journal of Biological Chemistry 285, 10078–10086. https://doi.org/10.1074/jbc.M109.034793

Chen, G., Trombley, P.Q., Van Den Pol, A.N., 1995. GABA receptors precede glutamate receptors in hypothalamic development; differential regulation by astrocytes. Journal of Neurophysiology 74, 1473–1484. https://doi.org/10.1152/jn.1995.74.4.1473

Chen, P.-F., Hsiao, J.S., Sirois, C.L., Chamberlain, S.J., 2016. RBFOX1 and RBFOX2 are dispensable in iPSCs and iPSC-derived neurons and do not contribute to neural-specific paternal UBE3A silencing. Sci Rep 6, 25368. https://doi.org/10.1038/srep25368

Chiang, C., Litingtung, Y., Lee, E., Young, K.E., Corden, J.L., Westphal, H., Beachy, P.A., 1996. Cyclopia and defective axial patterning in mice lacking Sonic hedgehog gene function. Nature 383, 407–413. https://doi.org/10.1038/383407a0

Cipollini, E., Riccio, M., Di Giaimo, R., Dal Piaz, F., Pulice, G., Catania, S., Caldarelli, I., Dembic, M., Santi, S., Melli, M., 2008. Cystatin B and its EPM1 mutants are polymeric and aggregate prone in vivo. Biochimica et Biophysica Acta (BBA) - Molecular Cell Research 1783, 312–322. https://doi.org/10.1016/j.bbamcr.2007.08.007

D'amato, E., Kokaia, Z., Nanobashvili, A., Reeben, M., Lehesjoki, A., Saarma, M., Lindvall, O., 2000. Seizures induce widespread upregulation of cystatin B, the gene mutated in progressive myoclonus epilepsy, in rat forebrain neurons. Eur J of Neuroscience 12, 1687–1695. https://doi.org/10.1046/j.1460-9568.2000.00058.x

Daura, E., Tegelberg, S., Hakala, P., Lehesjoki, A.-E., Joensuu, T., 2022. Cystatin B deficiency results in sustained histone H3 tail cleavage in postnatal mouse brain mediated by increased chromatin-associated cathepsin L activity. Front. Mol. Neurosci. 15, 1069122. https://doi.org/10.3389/fnmol.2022.1069122

Daura, E., Tegelberg, S., Yoshihara, M., Jackson, C., Simonetti, F., Aksentjeff, K., Ezer, S., Hakala, P., Katayama, S., Kere, J., Lehesjoki, A.-E., Joensuu, T., 2021. Cystatin B-deficiency triggers ectopic histone H3 tail cleavage during neurogenesis. Neurobiology of Disease 156, 105418. https://doi.org/10.1016/j.nbd.2021.105418

DeFelipe, J., 2011. The Evolution of the Brain, the Human Nature of Cortical Circuits, and Intellectual Creativity. Front. Neuroanat. 5. https://doi.org/10.3389/fnana.2011.00029

Di Giaimo, R., 2002. New insights into the molecular basis of progressive myoclonus epilepsy: a multiprotein complex with cystatin B. Human Molecular Genetics 11, 2941–2950. https://doi.org/10.1093/hmg/11.23.2941

Di Giaimo, R., Penna, E., Pizzella, A., Cirillo, R., Perrone-Capano, C., Crispino, M., 2020. Cross Talk at the Cytoskeleton–Plasma Membrane Interface: Impact on Neuronal Morphology and Functions. IJMS 21, 9133. https://doi.org/10.3390/ijms21239133

Di Matteo, F., Bonrath, R., Pravata, V., Schmidt, H., Ayo Martin, A.C., Di Giaimo, R., Menegaz, D., Riesenberg, S., De Vrij, F.M.S., Maccarrone, G., Holzapfel, M., Straub, T., Kushner, S.A., Robertson, S.P., Eder, M., Cappello, S., 2025. Neuronal hyperactivity in neurons derived from individuals with gray matter heterotopia. Nat Commun 16, 1737. https://doi.org/10.1038/s41467-025-56998-1

Di Matteo, F., Pipicelli, F., Kyrousi, C., Tovecci, I., Penna, E., Crispino, M., Chambery, A., Russo, R., Ayo-Martin, A.C., Giordano, M., Hoffmann, A., Ciusani, E., Canafoglia, L., Götz, M., Di Giaimo, R., Cappello, S., 2020. Cystatin B is essential for proliferation and interneuron migration in individuals with EPM 1 epilepsy. EMBO Mol Med 12, e11419. https://doi.org/10.15252/emmm.201911419

Dixson, A.C., Dawson, T.R., Di Vizio, D., Weaver, A.M., 2023. Context-specific regulation of extracellular vesicle biogenesis and cargo selection. Nat Rev Mol Cell Biol 24, 454–476. https://doi.org/10.1038/s41580-023-00576-0

Eyman, M., Cefaliello, C., Ferrara, E., De Stefano, R., Crispino, M., Giuditta, A., 2007. Synaptosomal protein synthesis is selectively modulated by learning. Brain Research 1132, 148–157. https://doi.org/10.1016/j.brainres.2006.11.025

Fauré, J., Lachenal, G., Court, M., Hirrlinger, J., Chatellard-Causse, C., Blot, B., Grange, J., Schoehn, G., Goldberg, Y., Boyer, V., Kirchhoff, F., Raposo, G., Garin, J., Sadoul, R., 2006. Exosomes are released by cultured cortical neurones. Molecular and Cellular Neuroscience 31, 642–648. https://doi.org/10.1016/j.mcn.2005.12.003

Forero, A., Pipicelli, F., Moser, S., Baumann, N., Grätz, C., Gonzalez Pisfil, M., Pfaffl, M.W., Pütz, B., Kielkowski, P., Cernilogar, F.M., Maccarrone, G., Di Giaimo, R., Cappello, S., 2024a. Extracellular vesicle-mediated trafficking of molecular cues during human brain development. Cell Reports 43, 114755. https://doi.org/10.1016/j.celrep.2024.114755

Forero, A., Pravata, V., Pipicelli, F., Soloperto, A., Di Matteo, F., Bekjarova, Z., Frenna, E., Canafoglia, L., Ragona, F., Maccarrone, G., Pisfil, M.G., Whal-Schott, C., Cernilogar, F.M., Eder, M., Di Giaimo, R., Cappello, S., 2024b. Intrinsic and extrinsic mechanisms alter neural cell fate specification in EPM1 Epilepsy. https://doi.org/10.1101/2024.11.20.624470

Franceschetti, S., Sancini, G., Buzzi, A., Zucchini, S., Paradiso, B., Magnaghi, G., Frassoni, C., Chikhladze, M., Avanzini, G., Simonato, M., 2007. A pathogenetic hypothesis of Unverricht–Lundborg disease onset and progression. Neurobiology of Disease 25, 675–685. https://doi.org/10.1016/j.nbd.2006.11.006

Frühbeis, C., Fröhlich, D., Kuo, W.P., Krämer-Albers, E.-M., 2013. Extracellular vesicles as mediators of neuron-glia communication. Front. Cell. Neurosci. 7. https://doi.org/10.3389/fncel.2013.00182

Fuccillo, M., Rallu, M., McMahon, A.P., Fishell, G., 2004. Temporal requirement for hedgehog signaling in ventral telencephalic patterning. Development 131, 5031–5040. https://doi.org/10.1242/dev.01349

Gestaut, D., Roh, S.H., Ma, B., Pintilie, G., Joachimiak, L.A., Leitner, A., Walzthoeni, T., Aebersold, R., Chiu, W., Frydman, J., 2019. The Chaperonin TRiC/CCT Associates with Prefoldin through a Conserved Electrostatic Interface Essential for Cellular Proteostasis. Cell 177, 751-765.e15. https://doi.org/10.1016/j.cell.2019.03.012

Gestaut, D., Zhao, Y., Park, J., Ma, B., Leitner, A., Collier, M., Pintilie, G., Roh, S.-H., Chiu, W., Frydman, J., 2023. Structural visualization of the tubulin folding pathway directed by human chaperonin TRiC/CCT. Cell 186, 2038. https://doi.org/10.1016/j.cell.2023.04.004

Ghozlan, H., Cox, A., Nierenberg, D., King, S., Khaled, A.R., 2022. The TRiCky Business of Protein Folding in Health and Disease. Front. Cell Dev. Biol. 10, 906530. https://doi.org/10.3389/fcell.2022.906530

Gilbert, L.A., Larson, M.H., Morsut, L., Liu, Z., Brar, G.A., Torres, S.E., Stern-Ginossar, N., Brandman, O., Whitehead, E.H., Doudna, J.A., Lim, W.A., Weissman, J.S., Qi, L.S., 2013. CRISPR-Mediated Modular RNA-Guided Regulation of Transcription in Eukaryotes. Cell 154, 442–451. https://doi.org/10.1016/j.cell.2013.06.044

Goldman, D.H., Kaiser, C.M., Milin, A., Righini, M., Tinoco, I., Bustamante, C., 2015. Mechanical force releases nascent chain–mediated ribosome arrest in vitro and in vivo. Science 348, 457–460. https://doi.org/10.1126/science.1261909

Gomes, A.R., Sangani, N.B., Fernandes, T.G., Diogo, M.M., Curfs, L.M.G., Reutelingsperger, C.P., 2020. Extracellular Vesicles in CNS Developmental Disorders. IJMS 21, 9428. https://doi.org/10.3390/ijms21249428

Gorski, K., Jackson, C.B., Nyman, T.A., Rezov, V., Battersby, B.J., Lehesjoki, A.-E., 2023. Progressive mitochondrial dysfunction in cerebellar synaptosomes of cystatin B-deficient mice. Front. Mol. Neurosci. 16, 1175851. https://doi.org/10.3389/fnmol.2023.1175851

Gorski, K., Spoljaric, A., Nyman, T.A., Kaila, K., Battersby, B.J., Lehesjoki, A.-E., 2020. Quantitative Changes in the Mitochondrial Proteome of

Cerebellar Synaptosomes From Preclinical Cystatin B-Deficient Mice. Front. Mol. Neurosci. 13, 570640. https://doi.org/10.3389/fnmol.2020.570640

Grantham, J., Brackley, K.I., Willison, K.R., 2006. Substantial CCT activity is required for cell cycle progression and cytoskeletal organization in mammalian cells. Experimental Cell Research 312, 2309–2324. https://doi.org/10.1016/j.yexcr.2006.03.028

Gunhanlar, N., Shpak, G., Van Der Kroeg, M., Gouty-Colomer, L.A., Munshi, S.T., Lendemeijer, B., Ghazvini, M., Dupont, C., Hoogendijk, W.J.G., Gribnau, J., De Vrij, F.M.S., Kushner, S.A., 2018. A simplified protocol for differentiation of electrophysiologically mature neuronal networks from human induced pluripotent stem cells. Mol Psychiatry 23, 1336–1344. https://doi.org/10.1038/mp.2017.56

Hagey, D.W., Ojansivu, M., Bostancioglu, B.R., Saher, O., Bost, J.P., Gustafsson, M.O., Gramignoli, R., Svahn, M., Gupta, D., Stevens, M.M., Görgens, A., El Andaloussi, S., 2023. The cellular response to extracellular vesicles is dependent on their cell source and dose. Sci. Adv. 9, eadh1168. https://doi.org/10.1126/sciadv.adh1168

Heng, J.I.-T., Chariot, A., Nguyen, L., 2010. Molecular layers underlying cytoskeletal remodelling during cortical development. Trends in Neurosciences 33, 38–47. https://doi.org/10.1016/j.tins.2009.09.003

Hetz, C., 2021. Adapting the proteostasis capacity to sustain brain healthspan. Cell 184, 1545–1560. https://doi.org/10.1016/j.cell.2021.02.007

Hodeify, R., Nandakumar, M., Own, M., Courjaret, R.J., Graumann, J., Hubrack, S.Z., Machaca, K., 2018. The CCT chaperonin is a novel regulator of Ca^{2+} signaling through modulation of Orai1 trafficking. Sci. Adv. 4, eaau1935. https://doi.org/10.1126/sciadv.aau1935

Hyppönen, J., Äikiä, M., Joensuu, T., Julkunen, P., Danner, N., Koskenkorva, P., Vanninen, R., Lehesjoki, A.-E., Mervaala, E., Kälviäinen, R., 2015. Refining the phenotype of Unverricht-Lundborg disease (EPM1): A population-wide Finnish study. Neurology 84, 1529–1536. https://doi.org/10.1212/WNL.0000000000001466

Jerala, R., Trstenjak, M., Lenarčič, B., Turk, V., 1988. Cloning a synthetic gene for human stefin B and its expression in *E. coli*. FEBS Letters 239, 41–44. https://doi.org/10.1016/0014-5793(88)80541-6

Jin, M., Liu, C., Han, W., Cong, Y., 2019. TRiC/CCT Chaperonin: Structure and Function, in: Harris, J.R., Marles-Wright, J. (Eds.), Macromolecular Protein Complexes II: Structure and Function, Subcellular Biochemistry. Springer International Publishing, Cham, pp. 625–654. https://doi.org/10.1007/978-3-030-28151-9_19

Joachimiak, L.A., Walzthoeni, T., Liu, C.W., Aebersold, R., Frydman, J., 2014. The Structural Basis of Substrate Recognition by the Eukaryotic Chaperonin TRiC/CCT. Cell 159, 1042–1055. https://doi.org/10.1016/j.cell.2014.10.042

Joensuu, T., Kuronen, M., Alakurtti, K., Tegelberg, S., Hakala, P., Aalto, A., Huopaniemi, L., Aula, N., Michellucci, R., Eriksson, K., Lehesjoki, A.-E., 2007. Cystatin B: mutation detection, alternative splicing and expression in progressive myclonus epilepsy of Unverricht-Lundborg type (EPM1) patients. Eur J Hum Genet 15, 185–193. https://doi.org/10.1038/sj.ejhg.5201723

Joensuu, T., Lehesjoki, A., Kopra, O., 2008. Molecular background of EPM1—Unverricht–Lundborg disease. Epilepsia 49, 557–563. https://doi.org/10.1111/j.1528-1167.2007.01422.x

Joensuu, T., Tegelberg, S., Reinmaa, E., Segerstråle, M., Hakala, P., Pehkonen, H., Korpi, E.R., Tyynelä, J., Taira, T., Hovatta, I., Kopra, O., Lehesjoki, A.-E., 2014. Gene Expression Alterations in the Cerebellum and Granule Neurons of Cstb−/− Mouse Are Associated with Early Synaptic Changes and Inflammation. PLoS ONE 9, e89321. https://doi.org/10.1371/journal.pone.0089321

Kaasik, A., Kuum, M., Aonurm, A., Kalda, A., Vaarmann, A., Zharkovsky, A., 2007. Seizures, Ataxia, and Neuronal Loss in Cystatin B Heterozygous Mice. Epilepsia 48, 752–757. https://doi.org/10.1111/j.1528-1167.2007.00985.x

Kälviäinen, R., Khyuppenen, J., Koskenkorva, P., Eriksson, K., Vanninen, R., Mervaala, E., 2008. Clinical picture of EPM1-Unverricht-Lundborg

disease. Epilepsia 49, 549–556. https://doi.org/10.1111/j.1528-1167.2008.01546.x

Khabirova, E., Moloney, A., Marciniak, S.J., Williams, J., Lomas, D.A., Oliver, S.G., Favrin, G., Sattelle, D.B., Crowther, D.C., 2014. The TRiC/CCT Chaperone Is Implicated in Alzheimer's Disease Based on Patient GWAS and an RNAi Screen in Aβ-Expressing Caenorhabditis elegans. PLoS ONE 9, e102985. https://doi.org/10.1371/journal.pone.0102985

Klaus, J., Kanton, S., Kyrousi, C., Ayo-Martin, A.C., Di Giaimo, R., Riesenberg, S., O'Neill, A.C., Camp, J.G., Tocco, C., Santel, M., Rusha, E., Drukker, M., Schroeder, M., Götz, M., Robertson, S.P., Treutlein, B., Cappello, S., 2019. Altered neuronal migratory trajectories in human cerebral organoids derived from individuals with neuronal heterotopia. Nat Med 25, 561–568. https://doi.org/10.1038/s41591-019-0371-0

Kopitar-Jerala, N., 2015. The Role of Stefin B in Neuro-inflammation. Front. Cell. Neurosci. 9. https://doi.org/10.3389/fncel.2015.00458

Kraft, F., Rodriguez-Aliaga, P., Yuan, W., Franken, L., Zajt, K., Hasan, D., Lee, T.-T., Flex, E., Hentschel, A., Innes, A.M., Zheng, B., Julia Suh, D.S., Knopp, C., Lausberg, E., Krause, J., Zhang, X., Trapane, P., Carroll, R., McClatchey, M., Fry, A.E., Wang, L., Giesselmann, S., Hoang, H., Baldridge, D., Silverman, G.A., Radio, F.C., Bertini, E., Ciolfi, A., Blood, K.A., De Sainte Agathe, J.-M., Charles, P., Bergant, G., Čuturilo, G., Peterlin, B., Diderich, K., Streff, H., Robak, L., Oegema, R., Van Binsbergen, E., Herriges, J., Saunders, C.J., Maier, A., Wolking, S., Weber, Y., Lochmüller, H., Meyer, S., Aleman, A., Polavarapu, K., Nicolas, G., Goldenberg, A., Guyant, L., Pope, K., Hehmeyer, K.N., Monaghan, K.G., Quade, A., Smol, T., Caumes, R., Duerinckx, S., Depondt, C., Van Paesschen, W., Rieubland, C., Poloni, C., Guipponi, M., Arcioni, S., Meuwissen, M., Jansen, A.C., Rosenblum, J., Haack, T.B., Bertrand, M., Gerstner, L., Magg, J., Riess, O., Schulz, J.B., Wagner, N., Wiesmann, M., Weis, J., Eggermann, T., Begemann, M., Roos, A., Häusler, M., Schedl, T., Tartaglia, M., Bremer, J., Pak, S.C., Frydman, J., Elbracht, M., Kurth, I., 2024. Brain malformations and seizures by impaired chaperonin function of TRiC. Science 386, 516–525. https://doi.org/10.1126/science.adp8721

Kubota, H., Hynes, G., Carne, A., Ashworth, A., Willison, K., 1994. Identification of six Tcp-1-related genes encoding divergent subunits of

the TCP-1-containing chaperonin. Current Biology 4, 89–99. https://doi.org/10.1016/S0960-9822(94)00024-2

Kyrousi, C., O'Neill, A.C., Brazovskaja, A., He, Z., Kielkowski, P., Coquand, L., Di Giaimo, R., D' Andrea, P., Belka, A., Forero Echeverry, A., Mei, D., Lenge, M., Cruceanu, C., Buchsbaum, I.Y., Khattak, S., Fabien, G., Binder, E., Elmslie, F., Guerrini, R., Baffet, A.D., Sieber, S.A., Treutlein, B., Robertson, S.P., Cappello, S., 2021. Extracellular LGALS3BP regulates neural progenitor position and relates to human cortical complexity. Nat Commun 12, 6298. https://doi.org/10.1038/s41467-021-26447-w

Lachenal, G., Pernet-Gallay, K., Chivet, M., Hemming, F.J., Belly, A., Bodon, G., Blot, B., Haase, G., Goldberg, Y., Sadoul, R., 2011. Release of exosomes from differentiated neurons and its regulation by synaptic glutamatergic activity. Molecular and Cellular Neuroscience 46, 409–418. https://doi.org/10.1016/j.mcn.2010.11.004

Lalioti, M.D., Scott, H.S., Buresi, C., Rossier, C., Bottani, A., Morris, M.A., Malafosse, A., Antonarakis, S.E., 1997. Dodecamer repeat expansion in cystatin B gene in progressive myoclonus epilepsy. Nature 386, 847–851. https://doi.org/10.1038/386847a0

Lancaster, M.A., Knoblich, J.A., 2014. Generation of cerebral organoids from human pluripotent stem cells. Nat Protoc 9, 2329–2340. https://doi.org/10.1038/nprot.2014.158

Lancaster, M.A., Renner, M., Martin, C.-A., Wenzel, D., Bicknell, L.S., Hurles, M.E., Homfray, T., Penninger, J.M., Jackson, A.P., Knoblich, J.A., 2013. Cerebral organoids model human brain development and microcephaly. Nature 501, 373–379. https://doi.org/10.1038/nature12517

Lehesjoki, A.-E., Kälviäinen, R., 1993. Progressive Myoclonic Epilepsy Type 1, in: Adam, M.P., Feldman, J., Mirzaa, G.M., Pagon, R.A., Wallace, S.E., Amemiya, A. (Eds.), GeneReviews®. University of Washington, Seattle, Seattle (WA).

Lehesjoki, A.-E., Koskiniemi, M., Pandolfo, M., Antonelli, A., Kyllerman, M., Wahlström, J., Nergårdh, A., Burmeister, M., Sistonen, P., Norio, R., De La Chapelle, A., 1992. Linkage studies in progressive myoclonus

epilepsy: Unverricht-Lundborg and Lafora's diseases. Neurology 42, 1545–1545. https://doi.org/10.1212/WNL.42.8.1545

Liliental, J., Chang, D.D., 1998. Rack1, a Receptor for Activated Protein Kinase C, Interacts with Integrin β Subunit. Journal of Biological Chemistry 273, 2379–2383. https://doi.org/10.1074/jbc.273.4.2379

Llorca, O., Martín-Benito, J., Gómez-Puertas, P., Ritco-Vonsovici, M., Willison, K.R., Carrascosa, J.L., Valpuesta, J.M., 2001. Analysis of the Interaction between the Eukaryotic Chaperonin CCT and Its Substrates Actin and Tubulin. Journal of Structural Biology 135, 205–218. https://doi.org/10.1006/jsbi.2001.4359

Llorca, O., McCormack, E.A., Hynes, G., Grantham, J., Cordell, J., Carrascosa, J.L., Willison, K.R., Fernandez, J.J., Valpuesta, J.M., 1999. Eukaryotic type II chaperonin CCT interacts with actin through specific subunits. Nature 402, 693–696. https://doi.org/10.1038/45294

Maas, S.L.N., Breakefield, X.O., Weaver, A.M., 2017. Extracellular Vesicles: Unique Intercellular Delivery Vehicles. Trends in Cell Biology 27, 172–188. https://doi.org/10.1016/j.tcb.2016.11.003

Macioce, P., Gandolfi, N., Leung, C.L., Chin, S.S.M., Malchiodi-Albedi, F., Ceccarini, M., Petrucci, T.C., Liem, R.K.H., 1999. Characterization of NF-L and βIIΣ1-Spectrin Interaction in Live Cells. Experimental Cell Research 250, 142–154. https://doi.org/10.1006/excr.1999.4479

Manninen, O., Koskenkorva, P., Lehtimäki, K.K., Hyppönen, J., Könönen, M., Laitinen, T., Kalimo, H., Kopra, O., Kälviäinen, R., Gröhn, O., Lehesjoki, A.-E., Vanninen, R., 2013. White Matter Degeneration with Unverricht-Lundborg Progressive Myoclonus Epilepsy: A Translational Diffusion-Tensor Imaging Study in Patients and Cystatin B–Deficient Mice. Radiology 269, 232–239. https://doi.org/10.1148/radiol.13122458

Martin-Cofreces, N.B., Valpuesta, J.M., Sánchez-Madrid, F., 2021. T cell asymmetry and metabolic crosstalk can fine-tune immunological synapses. Trends in Immunology 42, 649–653. https://doi.org/10.1016/j.it.2021.06.007

Marzesco, A.-M., Janich, P., Wilsch-Bräuninger, M., Dubreuil, V., Langenfeld, K., Corbeil, D., Huttner, W.B., 2005. Release of extracellular membrane particles carrying the stem cell marker prominin-1 (CD133)

from neural progenitors and other epithelial cells. Journal of Cell Science 118, 2849–2858. https://doi.org/10.1242/jcs.02439

Mittelbrunn, M., Vicente-Manzanares, M., Sánchez-Madrid, F., 2015. Organizing Polarized Delivery of Exosomes at Synapses. Traffic 16, 327–337. https://doi.org/10.1111/tra.12258

Okada, Y., Yamazaki, H., Sekine-Aizawa, Y., Hirokawa, N., 1995. The neuron-specific kinesin superfamily protein KIF1A is a uniqye monomeric motor for anterograde axonal transport of synaptic vesicle precursors. Cell 81, 769–780. https://doi.org/10.1016/0092-8674(95)90538-3

Okuneva, O., Körber, I., Li, Z., Tian, L., Joensuu, T., Kopra, O., Lehesjoki, A., 2015. Abnormal microglial activation in the *Cstb*$^{-/-}$ mouse, a model for progressive myoclonus epilepsy, EPM 1. Glia 63, 400–411. https://doi.org/10.1002/glia.22760

Okuneva, O., Li, Z., Körber, I., Tegelberg, S., Joensuu, T., Tian, L., Lehesjoki, A.-E., 2016. Brain inflammation is accompanied by peripheral inflammation in Cstb −/− mice, a model for progressive myoclonus epilepsy. J Neuroinflammation 13, 298. https://doi.org/10.1186/s12974-016-0764-7

Olivero, G., Cisani, F., Marimpietri, D., Di Paolo, D., Gagliani, M.C., Podestà, M., Cortese, K., Pittaluga, A., 2021. The Depolarization-Evoked, Ca2+-Dependent Release of Exosomes From Mouse Cortical Nerve Endings: New Insights Into Synaptic Transmission. Front. Pharmacol. 12, 670158. https://doi.org/10.3389/fphar.2021.670158

Orsini, A., Valetto, A., Bertini, V., Esposito, M., Carli, N., Minassian, B.A., Bonuccelli, A., Peroni, D., Michelucci, R., Striano, P., 2019. The best evidence for progressive myoclonic epilepsy: A pathway to precision therapy. Seizure 71, 247–257. https://doi.org/10.1016/j.seizure.2019.08.012

Paolicelli, R.C., Bergamini, G., Rajendran, L., 2019. Cell-to-cell Communication by Extracellular Vesicles: Focus on Microglia. Neuroscience 405, 148–157. https://doi.org/10.1016/j.neuroscience.2018.04.003

Patel, M.R., Weaver, A.M., 2021. Astrocyte-derived small extracellular vesicles promote synapse formation via fibulin-2-mediated TGF-β

signaling. Cell Reports 34, 108829.
https://doi.org/10.1016/j.celrep.2021.108829

Pavel, M., Imarisio, S., Menzies, F.M., Jimenez-Sanchez, M., Siddiqi, F.H., Wu, X., Renna, M., O'Kane, C.J., Crowther, D.C., Rubinsztein, D.C., 2016. CCT complex restricts neuropathogenic protein aggregation via autophagy. Nat Commun 7, 13821.
https://doi.org/10.1038/ncomms13821

Penna, E., Cerciello, A., Chambery, A., Russo, R., Cernilogar, F.M., Pedone, E.M., Perrone-Capano, C., Cappello, S., Di Giaimo, R., Crispino, M., 2019a. Cystatin B Involvement in Synapse Physiology of Rodent Brains and Human Cerebral Organoids. Front. Mol. Neurosci. 12, 195.
https://doi.org/10.3389/fnmol.2019.00195

Penna, E., Cerciello, A., Chambery, A., Russo, R., Cernilogar, F.M., Pedone, E.M., Perrone-Capano, C., Cappello, S., Di Giaimo, R., Crispino, M., 2019b. Cystatin B Involvement in Synapse Physiology of Rodent Brains and Human Cerebral Organoids. Front. Mol. Neurosci. 12, 195.
https://doi.org/10.3389/fnmol.2019.00195

Pennacchio, L.A., Lehesjoki, A.-E., Stone, N.E., Willour, V.L., Virtaneva, K., Miao, J., D'Amato, E., Ramirez, L., Faham, M., Koskiniemi, M., Warrington, J.A., Norio, R., De La Chapelle, A., Cox, D.R., Myers, R.M., 1996. Mutations in the Gene Encoding Cystatin B in Progressive Myoclonus Epilepsy (EPM1). Science 271, 1731–1734.
https://doi.org/10.1126/science.271.5256.1731

Pipicelli, F., Baumann, N., Di Giaimo, R., Forero-Echeverry, A., Kyrousi, C., Bonrath, R., Maccarrone, G., Jabaudon, D., Cappello, S., 2023. Non–cell-autonomous regulation of interneuron specification mediated by extracellular vesicles. Sci. Adv. 9, eadd8164.
https://doi.org/10.1126/sciadv.add8164

Pizzella, A., Penna, E., Abate, N., Frenna, E., Canafoglia, L., Ragona, F., Russo, R., Chambery, A., Perrone-Capano, C., Cappello, S., Crispino, M., Di Giaimo, R., 2024. Pathological Deficit of Cystatin B Impairs Synaptic Plasticity in EPM1 Human Cerebral Organoids. Mol Neurobiol 61, 4318–4334. https://doi.org/10.1007/s12035-023-03812-y

Prianichnikov, N., Koch, H., Koch, S., Lubeck, M., Heilig, R., Brehmer, S., Fischer, R., Cox, J., 2020. MaxQuant Software for Ion Mobility Enhanced Shotgun Proteomics. Molecular & Cellular Proteomics 19, 1058–1069. https://doi.org/10.1074/mcp.TIR119.001720

Que, Y., Qiu, Y., Ding, Z., Zhang, S., Wei, R., Xia, J., Lin, Y., 2024. The role of molecular chaperone CCT/TRiC in translation elongation: A literature review. Heliyon 10, e29029. https://doi.org/10.1016/j.heliyon.2024.e29029

Rakic, P., 2009. Evolution of the neocortex: a perspective from developmental biology. Nat Rev Neurosci 10, 724–735. https://doi.org/10.1038/nrn2719

Rallu, M., Machold, R., Gaiano, N., Corbin, J.G., McMahon, A.P., Fishell, G., 2002. Dorsoventral patterning is established in the telencephalon of mutants lacking both Gli3 and Hedgehog signaling. Development 129, 4963–4974. https://doi.org/10.1242/dev.129.21.4963

Raposo, G., Stoorvogel, W., 2013. Extracellular vesicles: Exosomes, microvesicles, and friends. Journal of Cell Biology 200, 373–383. https://doi.org/10.1083/jcb.201211138

Riccio, M., Santi, S., Dembic, M., Digiaimo, R., Cipollini, E., Costantinoceccarini, E., Ambrosetti, D., Maraldi, N., Melli, M., 2005. Cell-specific expression of the epm1 (cystatin B) gene in developing rat cerebellum. Neurobiology of Disease 20, 104–114. https://doi.org/10.1016/j.nbd.2005.02.012

Rojas-Gómez, A., Dosil, S.G., Chichón, F.J., Fernández-Gallego, N., Ferrarini, A., Calvo, E., Calzada-Fraile, D., Requena, S., Otón, J., Serrano, A., Tarifa, R., Arroyo, M., Sorrentino, A., Pereiro, E., Vázquez, J., Valpuesta, J.M., Sánchez-Madrid, F., Martín-Cófreces, N.B., 2023. Chaperonin CCT controls extracellular vesicle production and cell metabolism through kinesin dynamics. J of Extracellular Vesicle 12, 12333. https://doi.org/10.1002/jev2.12333

Saeedi, S., Israel, S., Nagy, C., Turecki, G., 2019. The emerging role of exosomes in mental disorders. Transl Psychiatry 9, 122. https://doi.org/10.1038/s41398-019-0459-9

Schiera, G., Di Liegro, C.M., Di Liegro, I., 2019. Cell-to-Cell Communication in Learning and Memory: From Neuro- and Glio-Transmission to Information Exchange Mediated by Extracellular Vesicles. IJMS 21, 266. https://doi.org/10.3390/ijms21010266

Schneider, C.A., Rasband, W.S., Eliceiri, K.W., 2012. NIH Image to ImageJ: 25 years of image analysis. Nat Methods 9, 671–675. https://doi.org/10.1038/nmeth.2089

Sha, Z., Brill, L.M., Cabrera, R., Kleifeld, O., Scheliga, J.S., Glickman, M.H., Chang, E.C., Wolf, D.A., 2009. The eIF3 Interactome Reveals the Translasome, a Supercomplex Linking Protein Synthesis and Degradation Machineries. Molecular Cell 36, 141–152. https://doi.org/10.1016/j.molcel.2009.09.026

Sharma, P., Mesci, P., Carromeu, C., McClatchy, D.R., Schiapparelli, L., Yates, J.R., Muotri, A.R., Cline, H.T., 2019. Exosomes regulate neurogenesis and circuit assembly. Proc. Natl. Acad. Sci. U.S.A. 116, 16086–16094. https://doi.org/10.1073/pnas.1902513116

Shen, L., Chen, C., Yang, A., Chen, Y., Liu, Q., Ni, J., 2015. Redox proteomics identification of specifically carbonylated proteins in the hippocampi of triple transgenic Alzheimer's disease mice at its earliest pathological stage. Journal of Proteomics 123, 101–113. https://doi.org/10.1016/j.jprot.2015.04.005

Sierra-Torre, V., Plaza-Zabala, A., Bonifazi, P., Abiega, O., Díaz-Aparicio, I., Tegelberg, S., Lehesjoki, A., Valero, J., Sierra, A., 2020. Microglial phagocytosis dysfunction in the dentate gyrus is related to local neuronal activity in a genetic model of epilepsy. Epilepsia 61, 2593–2608. https://doi.org/10.1111/epi.16692

Smalheiser, N.R., 2007. Exosomal transfer of proteins and RNAs at synapses in the nervous system. Biol Direct 2, 35. https://doi.org/10.1186/1745-6150-2-35

Solana-Balaguer, J., Campoy-Campos, G., Martín-Flores, N., Pérez-Sisqués, L., Sitjà-Roqueta, L., Kucukerden, M., Gámez-Valero, A., Coll-Manzano, A., Martí, E., Pérez-Navarro, E., Alberch, J., Soriano, J., Masana, M., Malagelada, C., 2023. Neuron-derived extracellular vesicles contain synaptic proteins, promote spine formation, activate TrkB-mediated

signalling and preserve neuronal complexity. J of Extracellular Vesicle 12, 12355. https://doi.org/10.1002/jev2.12355

Sot, B., Rubio-Muñoz, A., Leal-Quintero, A., Martínez-Sabando, J., Marcilla, M., Roodveldt, C., Valpuesta, J.M., 2017. The chaperonin CCT inhibits assembly of α-synuclein amyloid fibrils by a specific, conformation-dependent interaction. Sci Rep 7, 40859. https://doi.org/10.1038/srep40859

Takeda, Y.S., Xu, Q., 2015. Neuronal Differentiation of Human Mesenchymal Stem Cells Using Exosomes Derived from Differentiating Neuronal Cells. PLoS ONE 10, e0135111. https://doi.org/10.1371/journal.pone.0135111

Taverna, E., Götz, M., Huttner, W.B., 2014. The Cell Biology of Neurogenesis: Toward an Understanding of the Development and Evolution of the Neocortex. Annu. Rev. Cell Dev. Biol. 30, 465–502. https://doi.org/10.1146/annurev-cellbio-101011-155801

Tegelberg, S., Kopra, O., Joensuu, T., Cooper, J.D., Lehesjoki, A.-E., 2012. Early Microglial Activation Precedes Neuronal Loss in the Brain of the *Cstb*$^{-/-}$ Mouse Model of Progressive Myoclonus Epilepsy, EPM1. J Neuropathol Exp Neurol 71, 40–53. https://doi.org/10.1097/NEN.0b013e31823e68e1

Théry, C., Amigorena, S., Raposo, G., Clayton, A., 2006. Isolation and Characterization of Exosomes from Cell Culture Supernatants and Biological Fluids. CP Cell Biology 30. https://doi.org/10.1002/0471143030.cb0322s30

Théry, C., Witwer, K.W., Aikawa, E., Alcaraz, M.J., Anderson, J.D., Andriantsitohaina, R., Antoniou, A., Arab, T., Archer, F., Atkin-Smith, G.K., Ayre, D.C., Bach, J., Bachurski, D., Baharvand, H., Balaj, L., Baldacchino, S., Bauer, N.N., Baxter, A.A., Bebawy, M., Beckham, C., Bedina Zavec, A., Benmoussa, A., Berardi, A.C., Bergese, P., Bielska, E., Blenkiron, C., Bobis-Wozowicz, S., Boilard, E., Boireau, W., Bongiovanni, A., Borràs, F.E., Bosch, S., Boulanger, C.M., Breakefield, X., Breglio, A.M., Brennan, M.Á., Brigstock, D.R., Brisson, A., Broekman, M.L., Bromberg, J.F., Bryl-Górecka, P., Buch, S., Buck, A.H., Burger, D., Busatto, S., Buschmann, D., Bussolati, B., Buzás, E.I., Byrd, J.B., Camussi, G., Carter, D.R., Caruso, S., Chamley, L.W., Chang, Y., Chen, C., Chen, S., Cheng, L., Chin, A.R.,

Clayton, A., Clerici, S.P., Cocks, A., Cocucci, E., Coffey, R.J., Cordeiro-da-Silva, A., Couch, Y., Coumans, F.A., Coyle, B., Crescitelli, R., Criado, M.F., D'Souza-Schorey, C., Das, S., Datta Chaudhuri, A., De Candia, P., De Santana, E.F., De Wever, O., Del Portillo, H.A., Demaret, T., Deville, S., Devitt, A., Dhondt, B., Di Vizio, D., Dieterich, L.C., Dolo, V., Dominguez Rubio, A.P., Dominici, M., Dourado, M.R., Driedonks, T.A., Duarte, F.V., Duncan, H.M., Eichenberger, R.M., Ekström, K., El Andaloussi, S., Elie-Caille, C., Erdbrügger, U., Falcón-Pérez, J.M., Fatima, F., Fish, J.E., Flores-Bellver, M., Försönits, A., Frelet-Barrand, A., Fricke, F., Fuhrmann, G., Gabrielsson, S., Gámez-Valero, A., Gardiner, C., Gärtner, K., Gaudin, R., Gho, Y.S., Giebel, B., Gilbert, C., Gimona, M., Giusti, I., Goberdhan, D.C., Görgens, A., Gorski, S.M., Greening, D.W., Gross, J.C., Gualerzi, A., Gupta, G.N., Gustafson, D., Handberg, A., Haraszti, R.A., Harrison, P., Hegyesi, H., Hendrix, A., Hill, A.F., Hochberg, F.H., Hoffmann, K.F., Holder, B., Holthofer, H., Hosseinkhani, B., Hu, G., Huang, Y., Huber, V., Hunt, S., Ibrahim, A.G., Ikezu, T., Inal, J.M., Isin, M., Ivanova, A., Jackson, H.K., Jacobsen, S., Jay, S.M., Jayachandran, M., Jenster, G., Jiang, L., Johnson, S.M., Jones, J.C., Jong, A., Jovanovic-Talisman, T., Jung, S., Kalluri, R., Kano, S., Kaur, S., Kawamura, Y., Keller, E.T., Khamari, D., Khomyakova, E., Khvorova, A., Kierulf, P., Kim, K.P., Kislinger, T., Klingeborn, M., Klinke, D.J., Kornek, M., Kosanović, M.M., Kovács, Á.F., Krämer-Albers, E., Krasemann, S., Krause, M., Kurochkin, I.V., Kusuma, G.D., Kuypers, S., Laitinen, S., Langevin, S.M., Languino, L.R., Lannigan, J., Lässer, C., Laurent, L.C., Lavieu, G., Lázaro-Ibáñez, E., Le Lay, S., Lee, M., Lee, Y.X.F., Lemos, D.S., Lenassi, M., Leszczynska, A., Li, I.T., Liao, K., Libregts, S.F., Ligeti, E., Lim, R., Lim, S.K., Linē, A., Linnemannstöns, K., Llorente, A., Lombard, C.A., Lorenowicz, M.J., Lörincz, Á.M., Lötvall, J., Lovett, J., Lowry, M.C., Loyer, X., Lu, Q., Lukomska, B., Lunavat, T.R., Maas, S.L., Malhi, H., Marcilla, A., Mariani, J., Mariscal, J., Martens-Uzunova, E.S., Martin-Jaular, L., Martinez, M.C., Martins, V.R., Mathieu, M., Mathivanan, S., Maugeri, M., McGinnis, L.K., McVey, M.J., Meckes, D.G., Meehan, K.L., Mertens, I., Minciacchi, V.R., Möller, A., Møller Jørgensen, M., Morales-Kastresana, A., Morhayim, J., Mullier, F., Muraca, M., Musante, L., Mussack, V., Muth, D.C., Myburgh, K.H., Najrana, T., Nawaz, M., Nazarenko, I., Nejsum, P., Neri, C., Neri, T., Nieuwland, R., Nimrichter, L., Nolan, J.P., Nolte-'t Hoen, E.N., Noren Hooten, N., O'Driscoll, L., O'Grady, T., O'Loghlen, A., Ochiya, T., Olivier, M., Ortiz, A., Ortiz, L.A., Osteikoetxea, X., Østergaard, O., Ostrowski, M., Park, J.,

Pegtel, D.M., Peinado, H., Perut, F., Pfaffl, M.W., Phinney, D.G., Pieters, B.C., Pink, R.C., Pisetsky, D.S., Pogge Von Strandmann, E., Polakovicova, I., Poon, I.K., Powell, B.H., Prada, I., Pulliam, L., Quesenberry, P., Radeghieri, A., Raffai, R.L., Raimondo, S., Rak, J., Ramirez, M.I., Raposo, G., Rayyan, M.S., Regev-Rudzki, N., Ricklefs, F.L., Robbins, P.D., Roberts, D.D., Rodrigues, S.C., Rohde, E., Rome, S., Rouschop, K.M., Rughetti, A., Russell, A.E., Saá, P., Sahoo, S., Salas-Huenuleo, E., Sánchez, C., Saugstad, J.A., Saul, M.J., Schiffelers, R.M., Schneider, R., Schøyen, T.H., Scott, A., Shahaj, E., Sharma, S., Shatnyeva, O., Shekari, F., Shelke, G.V., Shetty, A.K., Shiba, K., Siljander, P.R., Silva, A.M., Skowronek, A., Snyder, O.L., Soares, R.P., Sódar, B.W., Soekmadji, C., Sotillo, J., Stahl, P.D., Stoorvogel, W., Stott, S.L., Strasser, E.F., Swift, S., Tahara, H., Tewari, M., Timms, K., Tiwari, S., Tixeira, R., Tkach, M., Toh, W.S., Tomasini, R., Torrecilhas, A.C., Tosar, J.P., Toxavidis, V., Urbanelli, L., Vader, P., Van Balkom, B.W., Van Der Grein, S.G., Van Deun, J., Van Herwijnen, M.J., Van Keuren-Jensen, K., Van Niel, G., Van Royen, M.E., Van Wijnen, A.J., Vasconcelos, M.H., Vechetti, I.J., Veit, T.D., Vella, L.J., Velot, É., Verweij, F.J., Vestad, B., Viñas, J.L., Visnovitz, T., Vukman, K.V., Wahlgren, J., Watson, D.C., Wauben, M.H., Weaver, A., Webber, J.P., Weber, V., Wehman, A.M., Weiss, D.J., Welsh, J.A., Wendt, S., Wheelock, A.M., Wiener, Z., Witte, L., Wolfram, J., Xagorari, A., Xander, P., Xu, J., Yan, X., Yáñez-Mó, M., Yin, H., Yuana, Y., Zappulli, V., Zarubova, J., Žėkas, V., Zhang, J., Zhao, Z., Zheng, L., Zheutlin, A.R., Zickler, A.M., Zimmermann, P., Zivkovic, A.M., Zocco, D., Zuba-Surma, E.K., 2018. Minimal information for studies of extracellular vesicles 2018 (MISEV2018): a position statement of the International Society for Extracellular Vesicles and update of the MISEV2014 guidelines. J of Extracellular Vesicle 7, 1535750. https://doi.org/10.1080/20013078.2018.1535750

Tyanova, S., Temu, T., Cox, J., 2016. The MaxQuant computational platform for mass spectrometry-based shotgun proteomics. Nat Protoc 11, 2301–2319. https://doi.org/10.1038/nprot.2016.136

Van Niel, G., D'Angelo, G., Raposo, G., 2018. Shedding light on the cell biology of extracellular vesicles. Nat Rev Mol Cell Biol 19, 213–228. https://doi.org/10.1038/nrm.2017.125

Verkhratsky, A., Matteoli, M., Parpura, V., Mothet, J., Zorec, R., 2016. Astrocytes as secretory cells of the central nervous system:

idiosyncrasies of vesicular secretion. The EMBO Journal 35, 239–257. https://doi.org/10.15252/embj.201592705

Vidal, M., Mangeat, P., Hoekstra, D., 1997. Aggregation reroutes molecules from a recycling to a vesicle-mediated secretion pathway during reticulocyte maturation. Journal of Cell Science 110, 1867–1877. https://doi.org/10.1242/jcs.110.16.1867

Virtaneva, K., D'Amato, E., Miao, J., Koskiniemi, M., Norio, R., Avanzini, G., Franceschetti, S., Michelucci, R., Tassinari, C.A., Omer, S., Pennacchio, L.A., Myers, R.M., Dieguez-Lucena, J.L., Krahe, R., Chapelle, A.D.L., Lehesjoki, A.-E., 1997. Unstable minisatellite expansion causing recessively inherited myoclonus epilepsy, EPM1. Nat Genet 15, 393–396. https://doi.org/10.1038/ng0497-393

Wang, Y.-Z., Castillon, C.C.M., Gebis, K.K., Bartom, E.T., d'Azzo, A., Contractor, A., Savas, J.N., 2024. Notch receptor-ligand binding facilitates extracellular vesicle-mediated neuron-to-neuron communication. Cell Reports 43, 113680. https://doi.org/10.1016/j.celrep.2024.113680

Whittaker, V.P., 1993. Thirty years of synaptosome research. J Neurocytol 22, 735–742. https://doi.org/10.1007/BF01181319

Xie, H., Hu, H., Chang, M., Huang, D., Gu, X., Xiong, X., Xiong, R., Hu, L., Li, G., 2016. Identification of chaperones in a MPP+-induced and ATRA/TPA-differentiated SH-SY5Y cell PD model. Am J Transl Res 8, 5659–5671.

Yam, A.Y., Xia, Y., Lin, H.-T.J., Burlingame, A., Gerstein, M., Frydman, J., 2008. Defining the TRiC/CCT interactome links chaperonin function to stabilization of newly made proteins with complex topologies. Nat Struct Mol Biol 15, 1255–1262. https://doi.org/10.1038/nsmb.1515

You, Y., Muraoka, S., Jedrychowski, M.P., Hu, J., McQuade, A.K., Young-Pearse, T., Aslebagh, R., Shaffer, S.A., Gygi, S.P., Blurton-Jones, M., Poon, W.W., Ikezu, T., 2022. Human neural cell type-specific extracellular vesicle proteome defines disease-related molecules associated with activated astrocytes in Alzheimer's disease brain. J of Extracellular Vesicle 11, e12183. https://doi.org/10.1002/jev2.12183

Žerovnik, E., 2022. Human stefin B: from its structure, folding, and aggregation to its function in health and disease. Front. Mol. Neurosci. 15, 1009976. https://doi.org/10.3389/fnmol.2022.1009976

Zhang, Z., Yu, K., You, Y., Jiang, P., Wu, Z., DeTure, M.A., Dickson, D.W., Ikezu, S., Peng, J., Ikezu, T., 2023. Comprehensive characterization of human brain-derived extracellular vesicles using multiple isolation methods: Implications for diagnostic and therapeutic applications. J of Extracellular Vesicle 12, 12358. https://doi.org/10.1002/jev2.12358

Zhao, X., Chen, X.-Q., Han, E., Hu, Y., Paik, P., Ding, Z., Overman, J., Lau, A.L., Shahmoradian, S.H., Chiu, W., Thompson, L.M., Wu, C., Mobley, W.C., 2016. TRiC subunits enhance BDNF axonal transport and rescue striatal atrophy in Huntington's disease. Proc. Natl. Acad. Sci. U.S.A. 113. https://doi.org/10.1073/pnas.1603020113

Zhou, J., Benito-Martin, A., Mighty, J., Chang, L., Ghoroghi, S., Wu, H., Wong, M., Guariglia, S., Baranov, P., Young, M., Gharbaran, R., Emerson, M., Mark, M.T., Molina, H., Canto-Soler, M.V., Selgas, H.P., Redenti, S., 2018. Retinal progenitor cells release extracellular vesicles containing developmental transcription factors, microRNA and membrane proteins. Sci Rep 8, 2823. https://doi.org/10.1038/s41598-018-20421-1

Zhou, J., Flores-Bellver, M., Pan, J., Benito-Martin, A., Shi, C., Onwumere, O., Mighty, J., Qian, J., Zhong, X., Hogue, T., Amponsah-Antwi, B., Einbond, L., Gharbaran, R., Wu, H., Chen, B.-J., Zheng, Z., Tchaikovskaya, T., Zhang, X., Peinado, H., Canto-Soler, M.V., Redenti, S., 2021. Human retinal organoids release extracellular vesicles that regulate gene expression in target human retinal progenitor cells. Sci Rep 11, 21128. https://doi.org/10.1038/s41598-021-00542-w

Zink, A., Lisowski, P., Prigione, A., 2021. Generation of Human iPSC-derived Neural Progenitor Cells (NPCs) as Drug Discovery Model for Neurological and Mitochondrial Disorders. BIO-PROTOCOL 11. https://doi.org/10.21769/BioProtoc.3939